

Elastic Plastic and Damage Model for Concrete Materials: Part I - Theoretical Formulation

George Z. Voyiadjis* and Ziad N. Taqieddin

Department of Civil and Environmental Engineering, Louisiana State University, Baton Rouge, LA 70803, USA

Abstract:

A thermodynamically consistent macroscopic constitutive model for concrete that incorporates concrete effective stress space plasticity and fracture energy based - continuum damage mechanics is presented. A plasticity yield criterion, with multiple hardening functions and a non-associative plastic flow rule, is used simultaneously with two (tensile and compressive) isotropic damage criteria. The spectral decomposition of the stress tensor into tensile and compressive components is utilized in all criteria in order to simulate different responses of the material under various loading patterns. The damage criteria are based on the hydrostatic-deviatoric sensitive damage energy release rates in tension and compression derived from the Helmholtz free energy function. Three dissipation mechanisms are defined, one for plasticity and two for damage, to control the dissipation process in the material model. The consistent elastic-plastic-damage tangent operator is also derived, which concludes the theoretical formulation of the proposed model. Verification examples are provided in order to evaluate the ability of the proposed model to capture the behavior of concrete under different states of loading. The detailed scheme of numerical integration of the constitutive equations and the application of the proposed model to study concrete and reinforced concrete members are important issues discussed in part II of this work

Keywords: Continuum Damage Mechanics, Concrete Plasticity Theory, Consistent Thermodynamics, Strain Equivalence Hypothesis, Consistent Damage-Elasto-Plastic Tangent Operator, Failure and Localization Analysis.

1. Introduction

Modeling the physical behavior of concrete materials in structural components remains as one of the most challenging fields in structural engineering. Sophisticated models are required in order to capture the nonlinearities that arise as the material is loaded. On the other hand, as the scope of a study reaches larger scales of structures, the complexity of those sophisticated models hinders the analysis and becomes an immense barrier between their theoretical elegance on one side and their implementation cost, applicability and convergence on the other. Therefore, the motivation of a study in this field should be the development of a consistent and rigorous approach to the constitutive modeling of concrete that is still simple to implement into Finite Elements (FE) codes, feasibly inexpensive to run, and capable of demonstrating convergence.

Throughout the years, different concepts involving plasticity theory and/or continuum damage mechanics have been used to simulate the experimentally observed behavior of concrete materials. Many efforts were presented by researchers to modify the classical theory of plasticity in order to make it more suitable for concrete materials by including the softening directly in the expression of a plastic yield surface by means of a hardening-softening function (Feenstra and de Borst, 1996; Bicanic and Pearce, 1996; Grassl et al., 2002; Park and Kim, 2005; and others). The plasticity-based approach was criticized for being unable to capture the stiffness degradation due to progressive damage growth; a drawback that has been debated in literature (e.g., Feenstra and de Borst, 1996).

Other researchers applied continuum damage mechanics to linear elastic analysis of concrete where the mechanical effect of the progressive microcracking and strain softening are represented by a set of internal state variables which act on the elastic behavior (Mazars, 1984; Mazars and Pijaudier-Cabot, 1989; Willam et al., 2001; Comi and Perego, 2001; Tao and Phillips, 2005; Labadi and Hannachi, 2005; Junior and Venturini, 2007; Khan et al., 2007). These elastic-damage models were successful in capturing the behavior of concrete under uniaxial loadings but many were criticized for being unable to model the plastic irreversible phenomena and their observed effects especially under more complicated loading combinations.

In order to capture the degradation of the elastic stiffness of the concrete material as well as its plastic irreversible deformations upon mechanical loading, the combined use of elastic-plastic constitutive equations along with continuum damage mechanics became vital to better describe the mechanical behavior of concrete. A brief literature survey reveals several possibilities for coupling plasticity and damage effects in a single constitutive relation.

*Email: voyiadjis@eng.lsu.edu

One way is to couple damage to concrete plasticity by defining damage growth as a function of plastic strains (e.g. Lubliner et. al., 1989; Oller et. al., 1990; Meschke and Lackner, 1997; Voyiadjis and Abu-Lebdeh, 1993, 1994; Abu-Lebdeh and Voyiadjis, 1993; Kratzig and Polling, 2004; and others). A difficulty arises however due to the fact that under uniaxial tension there is minor plastic effect and considerable damage growth, while under uniaxial compression, the situation is reversed with little damage and important plastic strains. In addition, it is not straight forward to explain how plastic strain may develop in concrete prior to microcracking. A common assumption is that irreversible strains are due to microcrack sliding and internal friction. Such a process requires the prior formation of internal surfaces, i.e., microcracks, (Jason et.al., 2006).

Another approach, that is more suited to both tension and compression responses of concrete, uses the effective stress space concept (Ju, 1989). The plastic yield function is written in the effective configuration pertaining to the stresses in the undamaged material. Many authors (Mazars and Pijaudier-Cabot, 1989; Yazdani and Schreyer, 1990; Hansen and Schreyer, 1992; Lee and Fenves, 1998, 2001; Faria et. al., 1998; Fichant et. al., 1999; Voyiadjis and Kattan, 1999, 2006; Jefferson, 2003; Salari et. al., 2004; Shen et. al., 2004; Jason et. al., 2006; Contrafatto and Cuomo, 2006; Cicekli et. al., 2007; Voyiadjis et. al., 2008b; Taqieddin, 2008) applied this approach to isotropic and anisotropic damage coupled to elasto-plasticity. It has been extended to other sources of damage, for instance, thermal damage as shown by Nechnech et. al. (2002) and Willam et. al. (2003).

A third possibility is the strong coupling approach. In contrary to the above where the plastic yield function is written in term of the effective stress, the actual (applied) stress appears in the plastic process, which becomes coupled to damage. The damage variables are coupled with the plastic deformation in the constitutive formulations which provide help in calibrating the parameters with the experimental results. Yet, the coupled relations are complex and result in an unstable numerical algorithm. This kind of algorithm may cause unrealistic representation of the plastic behavior of the concrete during numerical implementation and iteration procedures (Lee and Fenves, 1998). Luccioni et. al. (1996), Gatuingt and Pijaudier-Cabot (2002); and Voyiadjis et. al. (2008a) provided thermodynamic consistent backgrounds of such a model.

A thermodynamically consistent macroscopic elastic-plastic-damage constitutive approach is proposed here in an effort to model the nonlinear behavior of concrete materials. It is based on a fracture energy enhanced isotropic damage model, with tensile/ compressive damage criteria and parameters, combined with an effective stress space plasticity yield criterion with multiple hardening rules and a non-associative plasticity flow rule. The isotropic damage models the softening response and the decrease in the elastic stiffness, while hardening plasticity accounts for the development of irreversible strains and volumetric compressive behavior within the effective configuration.

The effective stress space concept is adopted here to provide a simple way to separate the damage and plastic processes in order to ease the numerical implementation into FE codes. An implicit/explicit approach is used, where the plastic part is implicit followed by an explicit damage part that depends on the updated effective stress and strain tensors. As a consequence, existing robust algorithms for integrating the constitutive relations can be implemented. The calibration of the material parameters is also easier to handle as a consequence of the separation of damage and plasticity processes.

The damage process here is elastic and strain controlled. The isotropic damage model proposed by Tao and Phillips (2005) will be modified here to better describe the damage behavior of concrete. While the Tao and Phillips (2005) model incorporated strain-softening in an elastic-damage framework without any fracture energy based coefficients (mesh sensitivity reduction coefficients), it is used in this work simultaneously with the effective stress space plasticity in order to describe damage irreversible phenomena in concrete materials. The plastic process shall be described using a yield function introduced by Lubliner et. al. (1989) and later modified by Lee and Fenves (1998) and Wu et. al. (2006). Fracture energy related coefficients (Feenstra and de Borst, 1996; Lee and Fenves, 1998; Wu et. al., 2006) are defined and incorporated in order to achieve a reasonable degree of discretization insensitivity in numerical calculations.

2. Elastic-Plastic-Damage Constitutive Relation

The model presented in this work is thermodynamically consistent and comes from a generalization of the effective stress space plasticity theory and isotropic continuum damage theory applied simultaneously under the assumptions of small strains, isothermal conditions and rate independence. The underlying mechanism to incorporate the effects of damage is provided by the hypothesis of strain equivalence (Steinmann et. al., 1994; Lemaitre and Chaboche, 1998; Voyiadjis and Kattan, 1999, 2006; Lammer and Tsakmakis, 2000; Menzel and Steinmann, 2003) between the intermediate configuration of multiplicative elastoplasticity and an additional fictitious or rather effective configuration (designated by an over-bar on top of the symbol). The hypothesis of strain equivalence states that the strains in the undamaged (effective) configuration are equal to the strains in the damaged counterpart, which can be expressed using the additive decomposition of the strain tensor into elastic and plastic parts as follows:

$$\left\{ \begin{array}{l} \varepsilon_{ij} = \varepsilon_{ij}^e + \varepsilon_{ij}^p \\ \bar{\varepsilon}_{ij} = \bar{\varepsilon}_{ij}^e + \bar{\varepsilon}_{ij}^p \end{array} \right\} \Rightarrow \varepsilon_{ij} = \bar{\varepsilon}_{ij} \quad (1)$$

The equivalence of the elastic strains will be used to obtain an expression for the elasticity tensor $E_{ijkl}(\Phi)$ in the damaged configuration, as well as the damage thermodynamic conjugate forces Y^\pm used in the damage yield criteria g^\pm . The equivalence of the plastic strains, on the other hand, will be justified through the use of the effective stress space plasticity (Ju, 1989) and the definition of the plastic Helmholtz free energy function. Both equivalences will be further discussed in a subsequent section.

By taking the time derivative of the arrangements in Eq. (1), the following strain rate equations necessary for the plastic-damage incremental procedure are obtained:

$$\left\{ \begin{array}{l} \dot{\varepsilon}_{ij} = \dot{\varepsilon}_{ij}^e + \dot{\varepsilon}_{ij}^p \\ \dot{\bar{\varepsilon}}_{ij} = \dot{\bar{\varepsilon}}_{ij}^e + \dot{\bar{\varepsilon}}_{ij}^p \end{array} \right\} \Rightarrow \dot{\varepsilon}_{ij} = \dot{\bar{\varepsilon}}_{ij} \quad (2)$$

The effective stress tensor (stresses in the undamaged configuration) can now be written in terms of the strain equivalence hypothesis and using Hook's law as:

$$\bar{\sigma}_{ij} = \bar{E}_{ijkl} \varepsilon_{kl}^e = \bar{E}_{ijkl} (\varepsilon_{kl} - \varepsilon_{kl}^p) \quad (3)$$

where \bar{E}_{ijkl} is the fourth-order isotropic elasticity tensor, also known as the undamaged elastic operator, given as:

$$\bar{E}_{ijkl} = 2\bar{G}I_{ijkl}^{dev} + \bar{K}\delta_{ij}\delta_{kl} \quad (4)$$

where $I_{ijkl}^{dev} = I_{ijkl} - \frac{1}{3}\delta_{ij}\delta_{kl}$ is the deviatoric part of the fourth-order identity tensor $I_{ijkl} = \frac{1}{2}(\delta_{ik}\delta_{jl} + \delta_{il}\delta_{jk})$, and \bar{G} and \bar{K} are the linear elastic shear and bulk moduli, respectively. The tensor δ_{ij} is the Kronecker delta, and is equal to one, $\delta_{ij} = 1$ when $i = j$ or zero, $\delta_{ij} = 0$ when $i \neq j$.

The rate of the stress tensor in the effective (undamaged) configuration can be written in terms of the strain equivalence hypothesis and Hook's law as:

$$\dot{\bar{\sigma}}_{ij} = \bar{E}_{ijkl} \dot{\varepsilon}_{kl}^e = \bar{E}_{ijkl} (\dot{\varepsilon}_{kl} - \dot{\varepsilon}_{kl}^p) \quad (5)$$

The damage configuration counterpart of Eq.(3), i.e. the stress tensor for the damaged material, is given as follows:

$$\sigma_{ij} = E_{ijkl}(\Phi) \varepsilon_{kl}^e = E_{ijkl}(\Phi) (\varepsilon_{kl} - \varepsilon_{kl}^p) \quad (6)$$

where E_{ijkl} is the fourth-order elasticity tensor dependent on the damage properties.

Applying the effective stress concept of Kachanov (1958), the Cauchy stress tensor σ_{ij} is related to the effective stress tensor $\bar{\sigma}_{ij}$ through the following expression:

$$\sigma_{ij} = (1 - \Phi) \bar{\sigma}_{ij} \quad (7)$$

The parameter Φ is the combined scalar damage variable defined here similar to that given by (Tao and Phillips, 2005):

$$\Phi = \frac{\llbracket \bar{\sigma}_{ij}^+ \rrbracket \varphi^+ + \llbracket \bar{\sigma}_{ij}^- \rrbracket \varphi^-}{\llbracket \bar{\sigma}_{ij} \rrbracket} \quad (8)$$

where φ^+ and φ^- are the tensile and compressive damage crack densities, respectively, $\bar{\sigma}_{ij}^+$ and $\bar{\sigma}_{ij}^-$ are the positive and negative spectral decomposition parts of the effective stress tensor, $\bar{\sigma}_{ij}$, obtained using the elastic-predictor plastic-corrector steps, and $\llbracket X_{ij} \rrbracket$ represents the scalar contraction of the second order tensor (an invariant), i.e., $\llbracket X_{ij} \rrbracket = X_{ij} X_{ij}$. This definition implies that damage under uniaxial loading is governed by the corresponding damage parameter, while

under bi-axial loading two damage parameters, φ^+ and φ^- , both contribute to the induced damage. Their effective contribution is in proportion to the ratio of positive and negative stress contractions to the total stress contraction. This definition is different than that given by Tao and Phillips (2005) where they avoided the decomposition of the stress tensor into positive and negative tensors by separating the principal values of the stress tensor into positive and negative values to further simplify the implementation in an FE code.

By substituting Eqs. (3) and (6) into Eq. (7), one obtains the following relations:

$$E_{ijkl} = (1 - \Phi) \bar{E}_{ijkl} \quad (9)$$

$$\sigma_{ij} = (1 - \Phi) \bar{E}_{ijkl} (\varepsilon_{kl} - \varepsilon_{kl}^p) \quad (10)$$

The expression for the fourth order elasticity tensor in the damaged configuration E_{ijkl} in terms of its effective counterpart \bar{E}_{ijkl} will also be derived from the elastic dissipation potential later on. The damage variable Φ has values from ranging from zero to one. The value $\Phi = 0$ corresponds to the undamaged (effective) material and the value $\Phi = 1$ corresponds to the fully damaged material. Damage associated with the failure mechanisms of the concrete (cracking and crushing) results in a reduction in the elastic stiffness (Eq.(9)). Within the context of the scalar-damage theory, the stiffness degradation is isotropic (i.e. the same damage evolution is assumed in different directions) and represented by a single degradation value Φ . The time derivative can now be applied to Eq. (10) to obtain the following constitutive relation for the elastic-plastic-damage model used in this work:

$$\dot{\sigma}_{ij} = (1 - \Phi) \bar{E}_{ijkl} \dot{\varepsilon}_{kl}^e - \dot{\Phi} \bar{E}_{ijkl} \varepsilon_{kl}^e \quad (11)$$

3. Consistent Thermodynamic Formulation

In this section, the thermodynamic framework of the elastic-plastic-damage formulation for concrete is developed. Irreversible thermodynamic following the internal variable procedure of Coleman and Gurtin (1967) will be applied. The internal variables and potentials used to describe the thermodynamic processes are introduced. The Lagrange minimization approach (calculus of functions of several variables) is used to derive the evolution equations for the proposed model. The constitutive equations are derived from the second law of thermodynamics, the expression of Helmholtz Free Energy (HFE), the additive decomposition of the total strain rate into elastic and plastic components, the Clausius-Duhem inequality, and the maximum dissipation principle.

The HFE can be expressed as a function of the following internal state variables characterizing the behavior of concrete both in tension and compression: the elastic strain tensor ε_{ij}^e , a set of plastic hardening variables (κ^+ , κ^-) defined here as the equivalent plastic strains in tension and compression, respectively, and the scalar damage variables (φ^+ and φ^-) representing the damage densities in the material under tension or compression, respectively, such that:

$$\psi = \psi (\varepsilon_{ij}^e, \kappa^+, \kappa^-, \varphi^+, \varphi^-) \quad (12)$$

The constitutive model proposed here is based on the hypothesis of uncoupled elasticity (e.g. Lubliner, 1990; Luccioni et. al., 1996; Faria et. al., 1998; Nechnech et. al., 2002; Salari et. al., 2004; Kratzig and Polling, 2004; Luccioni and Rougier, 2005; Shao et. al., 2006; Wu et. al., 2006). According to this hypothesis, the total free energy density per unit volume ψ can be assumed to be formed by two independent parts: an elastic part ψ^e and a plastic part ψ^p , corresponding to the elastic and plastic process respectively (both dissipative). Therefore, the HFE is given as:

$$\psi = \psi^e (\varepsilon_{ij}^e, \varphi^+, \varphi^-) + \psi^p (\kappa^+, \kappa^-) \quad (13)$$

It is assumed in the above decomposition that damage affects the elastic prosperities and not the plastic ones. This can be justified by the following: once micro-cracks are initiated during loading of a concrete material, local stresses are redistributed to undamaged material micro-bonds over the effective (undamaged) area. Thus, effective stresses of undamaged material points are higher than nominal stresses. Accordingly, it appears reasonable to state that the plastic flow occurs only in the undamaged material micro-bounds by means of effective quantities (Ju, 1989). The plastic response is therefore characterized in the effective stress space and the yield function is no longer written in term of the applied stress, rather, it is a function of the effective stress, i.e., the stress in the undamaged material in between the microcracks. This approach, which is more suited for brittle materials like concrete, has been extensively used by researchers (Simo and Ju, 1987a,b; Ju, 1989; Mazars and Pijaudier-Cabot, 1989; Yazdani and Schreyer, 1990; Hansen and Schreyer, 1992; Lee and Fenves, 1998; Faria et. al., 1998; Fichant et. al., 1999; Salari et. al., 2004; Jefferson, 2003;

Jason et. al., 2006; and others). This does not necessarily mean that the damage properties will not be affected by the plastic ones. As will be shown in the verification part of this work, the variation of the plastic behavior-related parameters will greatly affect the evolution of damage.

In the following, the thermodynamic conjugate forces associated with the internal state variables in Eqs. (12) or (13) are derived based on the second law of thermodynamics. For isothermal behavior, the second-law of thermodynamics states that the rate of change in the internal energy is less than or equal to the external expenditure of power such that:

$$\int_v \rho \dot{\psi} \, dv \leq P_{ext} \quad (14)$$

where P_{ext} is the external power which according to the principle of virtual power should be equal to the internal power such that:

$$P_{ext} = P_{int} = \int_v \sigma_{ij} \dot{\epsilon}_{ij} \, dv \quad (15)$$

Substituting Eq. (15) into Eq. (14), one obtains the following:

$$\int_v \rho \dot{\psi} \, dv - \int_v \sigma_{ij} \dot{\epsilon}_{ij} \, dv \leq 0 \quad \Leftrightarrow \quad \int_v (\rho \dot{\psi} - \sigma_{ij} \dot{\epsilon}_{ij}) \, dv \leq 0 \quad (16)$$

In a stepwise sense, the Clausius-Duhem inequality can be inferred from Eq. (16) as follows:

$$\sigma_{ij} \dot{\epsilon}_{ij} - \rho \dot{\psi} \geq 0 \quad (17)$$

Taking the time derivative of Eq. (13), the following expression can be written:

$$\dot{\psi} = \dot{\psi}^e + \dot{\psi}^p = \frac{\partial \psi^e}{\partial \epsilon_{ij}^e} \dot{\epsilon}_{ij}^e + \frac{\partial \psi^e}{\partial \phi^+} \dot{\phi}^+ + \frac{\partial \psi^e}{\partial \phi^-} \dot{\phi}^- + \frac{\partial \psi^p}{\partial \kappa^+} \dot{\kappa}^+ + \frac{\partial \psi^p}{\partial \kappa^-} \dot{\kappa}^- \quad (18)$$

By substituting the rate of the HFE density, Eq. (18), into the Clausius-Duhem inequality, Eq. (17), one can write the following relation:

$$\sigma_{ij} \dot{\epsilon}_{ij}^p + \left(\sigma_{ij} - \rho \frac{\partial \psi^e}{\partial \epsilon_{ij}^e} \right) \dot{\epsilon}_{ij}^e - \rho \frac{\partial \psi^e}{\partial \phi^+} \dot{\phi}^+ - \rho \frac{\partial \psi^e}{\partial \phi^-} \dot{\phi}^- - \rho \frac{\partial \psi^p}{\partial \kappa^+} \dot{\kappa}^+ - \rho \frac{\partial \psi^p}{\partial \kappa^-} \dot{\kappa}^- \geq 0 \quad (19)$$

The above equation is valid for any admissible internal state variable such that the Cauchy stress tensor can be define as:

$$\sigma_{ij} = \rho \frac{\partial \psi^e}{\partial \epsilon_{ij}^e} \quad (20)$$

and the non-negativeness of intrinsic dissipation can be written as:

$$\sigma_{ij} \dot{\epsilon}_{ij}^p + Y^+ \dot{\phi}^+ + Y^- \dot{\phi}^- - c^+ \dot{\kappa}^+ - c^- \dot{\kappa}^- \geq 0 \quad (21)$$

where the damage (Y^\pm) and plasticity (c^\pm) conjugate forces that appear in the above expression are defined as follows:

$$Y^+ = -\rho \frac{\partial \psi^e}{\partial \phi^+} \quad , \quad Y^- = -\rho \frac{\partial \psi^e}{\partial \phi^-} \quad , \quad c^+ = \rho \frac{\partial \psi^p}{\partial \kappa^+} \quad , \quad c^- = \rho \frac{\partial \psi^p}{\partial \kappa^-} \quad (22)\text{a-d}$$

The mechanical dissipation must satisfy the first (Clausius-Duhem) inequality of thermodynamics and can be decomposed in two parts: one part due to the plastic process Π^p and the other due to the damage process Π^d . The mechanical dissipation energy function Π can therefore be written as follows:

$$\Pi = \Pi^p + \Pi^d \geq 0 \quad (23)$$

The plasticity and damage dissipation potentials are given, respectively, as follows:

$$\Pi^p = \sigma_{ij} \dot{\epsilon}_{ij}^p - c^+ \dot{\kappa}^+ - c^- \dot{\kappa}^- \geq 0 \quad (24)$$

$$\Pi^d = Y^+ \dot{\phi}^+ + Y^- \dot{\phi}^- \geq 0 \quad (25)$$

The rate of the internal variables associated with plastic and damage deformations are obtained by utilizing the calculus of functions of several variables with the plasticity and damage Lagrange multipliers $\dot{\lambda}^p$ and $\dot{\lambda}_d^\pm$, respectively. Thus the following general objective function can be defined:

$$\Omega = \Pi - \dot{\lambda}^p F - \dot{\lambda}_d^+ g^+ - \dot{\lambda}_d^- g^- \geq 0 \quad (26)$$

where F and g^\pm are the plastic potential function and the tensile and compressive damage potential functions, respectively, to be defined later.

Use is now made of the well known maximum dissipation principle (Simo and Honein, 1990; Simo and Hughes, 1998), which describes the actual state of the thermodynamic forces $(\sigma_{ij}, Y^\pm, c^\pm)$ as the state that maximizes the dissipation function over all other possible admissible states. Hence, one can maximize the objective function Ω by using the following necessary conditions:

$$\frac{\partial \Omega}{\partial \sigma_{ij}} = 0, \quad \frac{\partial \Omega}{\partial Y^\pm} = 0, \quad \frac{\partial \Omega}{\partial c^\pm} = 0 \quad (27)$$

Substituting Eq. (26) into Eq. (27) along with Eqs. (24) and (25) yields the following thermodynamic laws corresponding to the conjugate forces (Eq. (22)):

$$\begin{aligned} \dot{\epsilon}_{ij}^p &= \dot{\lambda}^p \frac{\partial F^p}{\partial \sigma_{ij}}, \quad \dot{\phi}^+ = \dot{\lambda}_d^+ \frac{\partial g^+}{\partial Y^+}, \quad \dot{\phi}^- = \dot{\lambda}_d^- \frac{\partial g^-}{\partial Y^-} \\ \dot{\kappa}^+ &= \dot{\lambda}^p \frac{\partial F}{\partial c^+}, \quad \dot{\kappa}^- = \dot{\lambda}^p \frac{\partial F}{\partial c^-} \end{aligned} \quad (28)\text{a-e}$$

Note that Eq. (28) a is defined in terms of a plastic potential F^p different from F to indicate the use of a non-associative flow rule. It is also worthy to note that in this work, the damage criteria are characterized with scalar quantities – scalar thermodynamic conjugate forces and scalar damage parameter - therefore, the above general thermodynamic evolution laws for damage, Eqs. (28)b and (28)c, will be greatly simplified in the implementation procedure discussed in part II of this work.

4. The Helmholtz Free Energy Function

Based on the additive decomposition of the HFE function into elastic-damage and plastic parts discussed earlier, Eq.(13), this section introduces specific forms for the elastic-damage and plastic parts of the HFE function adopted in this work. The elastic-damage part of the HFE function will be defined first, followed by a definition for the plastic part.

The elastic-damage part of the HFE is defined using the spectral decomposition of the Cauchy stress tensor into tensile and compressive parts as well as the combined scalar damage variable, Φ , defined in Eq. (8).

To account for the different effects of damage mechanisms on the nonlinear performance of concrete under tension and compression, spectral decomposition (e.g. Ortiz, 1985; Ju, 1989; Lubliner et. al., 1989; Faria et. al., 1998; Lee and Fenves, 1998; Wu et. al., 2006) of the effective stress tensor $\bar{\sigma}_{ij}$ into positive and negative components $(\bar{\sigma}_{ij}^+, \bar{\sigma}_{ij}^-)$ is performed such that:

$$\bar{\sigma}_{ij} = \bar{\sigma}_{ij}^+ + \bar{\sigma}_{ij}^- \quad (29)$$

The total effective stress tensor $\bar{\sigma}_{ij}$ can be written in terms of its principal values $\hat{\sigma}^{(k)}$ and their corresponding principal directions $n_i^{(k)}$ ($k=1, 2, 3$) as follows:

$$\bar{\sigma}_{ij} = \sum_{k=1}^3 \hat{\sigma}^{(k)} n_i^{(k)} n_j^{(k)} = \hat{\sigma}^{(1)} n_i^{(1)} n_j^{(1)} + \hat{\sigma}^{(2)} n_i^{(2)} n_j^{(2)} + \hat{\sigma}^{(3)} n_i^{(3)} n_j^{(3)} \quad (30)$$

The positive part $\bar{\sigma}_{ij}^+$ can be obtained by considering only the tensile principal values as follows:

$$\bar{\sigma}_{ij}^+ = \sum_{k=1}^3 H(\hat{\sigma}^{(k)}) \hat{\sigma}^{(k)} n_i^{(k)} n_j^{(k)} \quad (31)$$

where H is the Heaviside step function (H = 1 for $\hat{\sigma}_{\max} > 0$ and H = 0 for $\hat{\sigma}_{\max} < 0$).

The principal stresses $\hat{\sigma}^{(k)}$ in Eqs. (30) and (31) are defined in the following form:

$$\hat{\sigma}^{(k)} = n_p^{(k)} \bar{\sigma}_{pq} n_q^{(k)} \quad (32)$$

By substituting Eq. (32) into Eq. (31), the tensile stress can be written as:

$$\bar{\sigma}_{ij}^+ = \sum_{k=1}^3 H(\hat{\sigma}^{(k)}) n_p^{(k)} \bar{\sigma}_{pq} n_q^{(k)} n_i^{(k)} n_j^{(k)} \quad (33)$$

The above equation can be rewritten as follows:

$$\bar{\sigma}_{ij}^+ = P_{ijpq}^+ \bar{\sigma}_{pq} \quad (34)$$

where

$$P_{ijpq}^+ = \sum_{k=1}^3 H(\hat{\sigma}^{(k)}) n_i^{(k)} n_j^{(k)} n_p^{(k)} n_q^{(k)} \quad (35)$$

and substituting Eq. (34) into Eq. (29), the following expressions are obtained:

$$\begin{aligned} \bar{\sigma}_{ij} &= P_{ijpq}^+ \bar{\sigma}_{pq} + \bar{\sigma}_{ij}^- \\ \bar{\sigma}_{ij}^- &= \bar{\sigma}_{ij} - P_{ijpq}^+ \bar{\sigma}_{pq} = [I_{ijpq} - P_{ijpq}^+] \bar{\sigma}_{pq} = P_{ijpq}^- \bar{\sigma}_{pq} \\ I_{ijpq} &= P_{ijpq}^+ + P_{ijpq}^- \end{aligned} \quad (36)$$

where P_{ijpq}^+ and P_{ijpq}^- are the tensile and compressive fourth-order projection tensors, respectively.

Next, the effective or undamaged elastic free energy $\rho\bar{\psi}^e$ of the concrete material is expressed as follows:

$$\rho\bar{\psi}^e = \frac{1}{2} \bar{\varepsilon}_{ij}^e \bar{E}_{ijkl} \bar{\varepsilon}_{kl}^e = \frac{1}{2} \bar{\sigma}_{ij}^e \bar{\varepsilon}_{ij}^e \quad (37)$$

In order to account for the stiffness degradation induced by the concrete material damage, the elastic free energy in the damaged configuration can be written in terms of the elastic strain equivalence hypothesis as follows:

$$\rho\psi^e = (1 - \Phi) \rho\bar{\psi}^e = \frac{1}{2} \varepsilon_{ij}^e E_{ijkl}(\Phi) \varepsilon_{kl}^e = \frac{1}{2} (1 - \Phi) \varepsilon_{ij}^e \bar{E}_{ijkl} \varepsilon_{kl}^e = \frac{1}{2} \sigma_{ij}^e \varepsilon_{ij}^e \quad (38)$$

The previous equation can be substituted into Eq. (20) to give the constitutive stress strain relation in the damaged configuration, Eq. (10). It also shows that the elasticity tensor in the damaged configuration $E_{ijkl}(\Phi)$ is given in terms of the elasticity tensor in the effective configuration \bar{E}_{ijkl} as shown in Eq. (9).

Experimental evidence (Resende, 1987) demonstrates that the susceptibility of concrete to damage and failure is different under pure hydrostatic loading than under deviatoric loading. Therefore, and in order to distinguish the different contributions of hydrostatic and deviatoric stress/strain components to damage, the above potential is separated into two parts and written as:

$$\rho\psi^e = \frac{1}{2} (1 - \Phi) (e_{ij}^e + \frac{1}{3} \varepsilon_{mm}^e \delta_{ij}) \bar{E}_{ijkl} (e_{kl}^e + \frac{1}{3} \varepsilon_{nn}^e \delta_{kl}) \quad (39)$$

In the above equation, the elastic strain tensor, ε_{uv}^e , has been additively decomposed into deviatoric, e_{uv}^e , and hydrostatic, $\frac{1}{3} \varepsilon_{pp}^e$, parts such that:

$$\varepsilon_{uv}^e = e_{uv}^e + \frac{1}{3} \varepsilon_{pp}^e \delta_{uv} \quad (40)$$

Expanding the above equation, one obtains the following:

$$\rho\psi^e = \frac{1}{2}(1-\Phi)(e_{ij}^e \bar{E}_{ijkl} e_{kl}^e + \frac{1}{3}\varepsilon_{nn}^e e_{ij}^e \bar{E}_{ijkl} \delta_{kl} + \frac{1}{3}\varepsilon_{mm}^e \delta_{ij} \bar{E}_{ijkl} e_{kl}^e + \frac{1}{9}(\varepsilon_{mm}^e)^2 \delta_{ij} \bar{E}_{ijkl} \delta_{kl}) \quad (41)$$

The term involving pure hydrostatic strains can be isolated from the rest of the terms as follows:

$$\rho\psi^e = \frac{1}{2}(1-\Phi)(e_{ij}^e \bar{E}_{ijkl} e_{kl}^e + \frac{1}{3}\varepsilon_{nn}^e e_{ij}^e \bar{E}_{ijkl} \delta_{kl} + \frac{1}{3}\varepsilon_{mm}^e \delta_{ij} \bar{E}_{ijkl} e_{kl}^e) + \frac{1}{2}(1-\Phi)(\frac{1}{9}(\varepsilon_{mm}^e)^2 \delta_{ij} \bar{E}_{ijkl} \delta_{kl}) \quad (42)$$

To reduce the susceptibility of the hydrostatic part to damage, Tao and Phillips (2005) used a damage multiplier χ in the term involving pure hydrostatic strain, $\frac{1}{18}(1-\Phi)(\varepsilon_{mm}^e)^2 \delta_{ij} \bar{E}_{ijkl} \delta_{kl}$, as follows:

$$\rho\psi^e = \frac{1}{2}(1-\Phi)(e_{ij}^e \bar{E}_{ijkl} e_{kl}^e + \frac{1}{3}\varepsilon_{nn}^e e_{ij}^e \bar{E}_{ijkl} \delta_{kl} + \frac{1}{3}\varepsilon_{mm}^e \delta_{ij} \bar{E}_{ijkl} e_{kl}^e) + \frac{1}{2}(1-\chi\Phi)(\frac{1}{9}(\varepsilon_{mm}^e)^2 \delta_{ij} \bar{E}_{ijkl} \delta_{kl}) \quad (43)$$

Considering the last term in the previous equation, the following manipulation can be performed in order to reach an objective result:

$$\begin{aligned} \frac{1}{2}(1-\chi\Phi)(\frac{1}{9}(\varepsilon_{mm}^e)^2 \delta_{ij} \bar{E}_{ijkl} \delta_{kl}) &= \frac{1}{2}(1-\overbrace{\Phi}^{Zero} + \Phi - \chi\Phi)(\frac{1}{9}(\varepsilon_{mm}^e)^2 \delta_{ij} \bar{E}_{ijkl} \delta_{kl}) \\ &= \left[\frac{1}{2}(1-\Phi) + \frac{1}{2}(\Phi - \chi\Phi) \right] (\frac{1}{9}(\varepsilon_{mm}^e)^2 \delta_{ij} \bar{E}_{ijkl} \delta_{kl}) \\ &= \left[\frac{1}{2}(1-\Phi) + \frac{1}{2}(1-\chi)\Phi \right] (\frac{1}{9}(\varepsilon_{mm}^e)^2 \delta_{ij} \bar{E}_{ijkl} \delta_{kl}) \end{aligned} \quad (44)$$

Substituting the final term in the above equation to Eq. (43), one obtains the following relation:

$$\rho\psi^e = \frac{1}{2}(1-\Phi)(e_{ij}^e \bar{E}_{ijkl} e_{kl}^e + \frac{1}{3}\varepsilon_{nn}^e e_{ij}^e \bar{E}_{ijkl} \delta_{kl} + \frac{1}{3}\varepsilon_{mm}^e \delta_{ij} \bar{E}_{ijkl} e_{kl}^e + \frac{1}{9}(\varepsilon_{mm}^e)^2 \delta_{ij} \bar{E}_{ijkl} \delta_{kl}) + \frac{1}{2}(1-\chi)\Phi(\frac{1}{9}(\varepsilon_{mm}^e)^2 \delta_{ij} \bar{E}_{ijkl} \delta_{kl}) \quad (45)$$

Comparing the above equation with Eq. (41), it can be seen that the first term on the right hand side of Eq. (45) is identical to the right hand side of Eq. (41), therefore, the elastic free energy function can be now written in terms of the total strain tensor and the hydrostatic strain tensor with the effect reduction factor, β , as follows:

$$\rho\psi^e = \frac{1}{2}(1-\Phi)\varepsilon_{ij}^e \bar{E}_{ijkl} \varepsilon_{kl}^e + \frac{1}{2}(1-\chi)\Phi(\frac{1}{9}(\varepsilon_{mm}^e)^2 \delta_{ij} \bar{E}_{ijkl} \delta_{kl}) \quad (46)$$

Based on the failure characteristics of concrete and the experimental fact that the effect of the hydrostatic strain component on damage is less than that of the deviatoric component, Tao and Phillips (2005) designed the damage multiplier (or damage reduction factor) χ to provide this reduction effect. Clearly, χ is less than or equal to one ($0 \leq \chi \leq 1$). For the uniaxial version, they defined the damage multiplier χ as the ratio of the average stress $\sigma_{mm}/3$ to the maximum principal stress $\hat{\sigma}_1$, i.e., $|\sigma_{mm}/3|/\hat{\sigma}_1$. Whereas, under bi-axial loadings, the response of concrete is dependent on the stress ratio, and since a relationship between damage and stress ratios is not straightforward to establish and due to the fact that no matter what the stress ratios are, it is with no doubt that material damage is the consequence of energy dissipation from the damage mechanics point of view, consequently, the bi-axial version of the damage multiplier χ is proposed to be a damage energy release rate, Y , dependent parameter (Tao and Phillips, 2005).

Different mathematical forms of the damage multiplier can be assumed as long as they can match the corresponding experimental data. Tao and Phillips (2005) adopted the following form of the damage reduction factor χ :

$$\chi = 1 - \frac{1}{1 + cY \exp(-dY)} \quad (47)$$

where (\exp) is the base of natural logarithms, and c and d can be regarded as two material constants to make χ dimensionless and be determined so as to match the experimental data. It is worth mentioning here that this form of the damage reduction factor introduces nonlinearity to the definition of the damage energy release rate (damage conjugate force) Y , and requires local iterations when solving for that damage release rate during a given strain increment. In this work, two reduction factors χ^\pm are used to correspond to the different tensile and compressive responses of the material to hydrostatic stresses.

Based on the thermodynamic framework, one can obtain expressions for the damage thermodynamic conjugate forces Y^+ and Y^- from Eqs. (46), (22)a, and (22)b in the following form:

$$Y^+ = -\rho \frac{\partial \psi^e}{\partial \varphi^+} = \frac{1}{2} \frac{\|\sigma_{ij}^+\|}{\|\sigma_{ij}\|} \left(\varepsilon_{ij}^e \bar{E}_{ijkl} \varepsilon_{kl}^e - \frac{1}{9} (1 - \chi^+) (\varepsilon_{mm}^e)^2 \delta_{ij} \bar{E}_{ijkl} \delta_{kl} \right) \quad (48)$$

$$Y^- = -\rho \frac{\partial \psi^e}{\partial \varphi^-} = \frac{1}{2} \frac{\|\sigma_{ij}^-\|}{\|\sigma_{ij}\|} \left(\varepsilon_{ij}^e \bar{E}_{ijkl} \varepsilon_{kl}^e - \frac{1}{9} (1 - \chi^-) (\varepsilon_{mm}^e)^2 \delta_{ij} \bar{E}_{ijkl} \delta_{kl} \right) \quad (49)$$

Since the magnitudes of the damage thermodynamic conjugate forces Y^+ and Y^- are measures of the susceptibility of the material to damage, the damage energy release rates Y^\pm are therefore used to define the damage criteria g^\pm in tension or compression, respectively.

The plastic part of the HFE is postulated to be a function of the plastic variables κ^+ and κ^- in the following form:

$$\rho \psi^p = f_0^+ \kappa^+ + \frac{1}{2} h (\kappa^+)^2 + f_0^- \kappa^- + Q \left(\kappa^- + \frac{1}{\omega} \exp(-\omega \kappa^-) \right) \quad (50)$$

where f_0^+ and f_0^- are the uniaxial tensile and compressive yield stresses, respectively. The hardening parameters κ^+ and κ^- are introduced as the equivalent plastic strains under tension and compression, respectively, defined as:

$$\kappa^+ = \int_0^t \dot{\kappa}^+ dt \quad (51)$$

$$\kappa^- = \int_0^t \dot{\kappa}^- dt \quad (52)$$

where $\dot{\kappa}^+$ and $\dot{\kappa}^-$ are the tensile and compressive equivalent plastic strain rates, respectively, which are assumed to be evaluated according to the following expressions (Lee and Fenves, 1998):

$$\dot{\kappa}^+ = r(\hat{\sigma}_i) \hat{e}_{\max}^p \quad (53)$$

$$\dot{\kappa}^- = -(1 - r(\hat{\sigma}_i)) \hat{e}_{\min}^p \quad (54)$$

where \hat{e}_{\max}^p and \hat{e}_{\min}^p are the maximum and minimum eigenvalues of the plastic strain rate tensor \dot{e}_{ij}^p such that $\hat{e}_1^p > \hat{e}_2^p > \hat{e}_3^p$ and $\hat{e}_{\max}^p = \hat{e}_1^p$ and $\hat{e}_{\min}^p = \hat{e}_3^p$. It should be mentioned here that the procedure for obtaining the eigenvalues of a second-order tensor (e.g. stress or strain) is a built-in function in ABAQUS readily available for the UMAT subroutine. Under uniaxial loading, these eigenvalues reduce to $\hat{e}_{\max}^p = \dot{e}_{11}^p$ in tension and $\hat{e}_{\min}^p = \dot{e}_{33}^p$ in compression. The dimensionless parameter $r(\hat{\sigma}_i)$ is a weight factor $0 \leq r(\hat{\sigma}_i) \leq 1$ depending on the effective principal stresses $\hat{\sigma}_i$ ($i = 1, 2, 3$) and is defined as follows (Lee and Fenves, 1998):

$$r(\hat{\sigma}_i) = \frac{\sum_{i=1}^3 \langle \hat{\sigma}_i \rangle}{\sum_{i=1}^3 |\hat{\sigma}_i|} \quad (55)$$

The symbol $\langle x \rangle$ is the Macauley bracket, defined as $\langle x \rangle = \frac{1}{2}(|x| + x)$. Note that $r(\hat{\sigma}_i)$ is equal to one if all the eigenstresses $\hat{\sigma}_i$ are positive and accordingly equal to zero if they are all negative. The parameters Q and ω are material constants related to the isotropic hardening function of the material.

Substituting Eq. (50) into Eqs. (22)a and (22)b yields the following expressions for the plasticity conjugate forces c^+ and c^- (the tensile and compressive hardening functions):

$$c^+ = \rho \frac{\partial \psi^p}{\partial \kappa^+} = f_0^+ + h \kappa^+ \quad (56)$$

and

$$c^- = \rho \frac{\partial \psi^p}{\partial \kappa^-} = f_0^- + Q [1 - \exp(-\omega \kappa^-)] \quad (57)$$

such that by taking the time derivative of the above two expressions, one can easily obtain the following evolution equations of the hardening functions c^+ and c^- in terms of the plastic internal state variables κ^+ and κ^- :

$$\dot{c}^+ = h \dot{\kappa}^+ \quad (58)$$

$$\dot{c}^- = \omega(Q - c_i^-) \dot{\kappa}^- \quad (59)$$

Equation (59) can be obtained by realizing that the exponential term, $\exp(-\omega \kappa^-)$, in the rate equation, $\dot{c}^- = \omega Q (\exp(-\omega \kappa^-)) \dot{\kappa}^-$, can be replaced by the following term, $\exp(-\omega \kappa^-) = 1 - \frac{c^- - f_0^-}{Q} = 1 - \frac{c_i^-}{Q}$, obtained from rearranging Eq. (57).

5. Plasticity Formulation

In this section, the effective stress space plasticity and its components will be discussed. Owing to the coupling between the damage evolutions and the plastic flow in the elastic plastic damage models, the so-called (effective stress space plasticity) was introduced by Ju (1989). In this approach the effective (undamaged) configuration is used in order to establish the evolution laws for the plastic strains governing the plastic irreversible behavior in the material (Wu et. al., 2006). To determine the required effective stress tensor $\bar{\sigma}_{ij}$, the evolution law for the irreversible plastic strains tensor ε_{ij}^p has to be established first. The additive decomposition of the effective total strain tensor into elastic and plastic parts is assumed, Eq. (1). An effective stress plasticity yield criterion with multiple hardening rules is used along with a non-associative flow rule. Both take into account the dilatation effect of concrete materials. A Kuhn-Tucker consistency condition is applied to obtain the evolution of the magnitude of plastic strains.

A crucial component of any material model that involves plasticity theory is the yield surface/criterion. This criterion should address and model the experimentally observed non-symmetrical behavior of concrete under tensile and compressive loadings. Assuming the same yield behavior for both tension and compression in concrete materials leads to over/under estimation of plastic deformations (Lubliner et. al., 1989). The yield criterion adopted in this work was first introduced in the Barcelona model by Lubliner et. al. (1989), and later modified by Lee and Fenves (1998, 2001) and Wu et. al. (2006). These works reported that the yield criterion is successful in simulating the concrete behavior under uniaxial, biaxial, multiaxial, and cyclic loading. This criterion is given in the effective stress space and expressed using the undamaged configuration parameters as follows:

$$f = \sqrt{3\bar{J}_2} + \alpha \bar{I}_1 + \beta (\kappa^\pm) H(\hat{\sigma}_{\max}) \hat{\sigma}_{\max} - (1 - \alpha) c^-(\kappa^-) = 0 \quad (60)$$

where $\bar{J}_2 = \bar{s}_{ij} \bar{s}_{ij} / 2$ is the second-invariant of the effective deviatoric stress $\bar{s}_{ij} = \bar{\sigma}_{ij} - \bar{\sigma}_{kk} \delta_{ij} / 3$, $\bar{I}_1 = \bar{\sigma}_{kk}$ is the first-invariant of the effective stress $\bar{\sigma}_{ij}$, κ^\pm denote a suitable set of plastic variables (Wu et. al., 2006) given as the equivalent plastic strains defined in Eqs. (53) and (54), $H(\hat{\sigma}_{\max})$ is the Heaviside step function defined in Eq.(31), and $\hat{\sigma}_{\max}$ is the maximum principal stress.

The parameter α is a dimensionless constant given by Lubliner et. al. (1989) as follows:

$$\alpha = \frac{(f_{b0}^- / f_0^-) - 1}{2(f_{b0}^- / f_0^-) - 1} \quad (61)$$

and the parameter β , defined as a constant in the Barcelona model, was later modified by Lee and Fenves (1998), and given as a dimensionless function of the tensile and compressive cohesions c^\pm (hardening internal state variables) in the following form:

$$\beta(\kappa^\pm) = (1 - \alpha) \frac{c^-(\kappa^-)}{c^+(\kappa^+)} - (1 + \alpha) \quad (62)$$

where f_{b0}^- and f_0^- are the initial equibiaxial and uniaxial compressive yield stresses, respectively. Experimental values of the ratio f_{b0}^- / f_0^- lie between 1.10 – 1.20 (Wu et. al., 2006); yielding α to be between 0.08 – 0.14. For further details about the derivation of both parameters, α and β , the reader is referred to Lubliner et. al. (1989).

The cohesion parameters, c^+ and c^- , denote evolution stresses (positive quantities) in the effective stress space due to plastic hardening under uniaxial tension and compression, respectively. They are defined as cohesion parameters due to the fact that concrete material behavior resembles that of a frictional material with cohesion (Lubliner et. al., 1989). Since the concrete behavior in compression is more of a ductile behavior, the compressive isotropic hardening function c^- is defined by the following exponential law:

$$c^-(\kappa^-) = f_0^- + Q [1 - \exp(-\omega \kappa^-)] \quad (63)$$

where Q and ω are material constants characterizing the saturated stress and the rate of saturation, respectively. On the other hand, a linear expression is assumed for the tensile hardening function c^+ such that:

$$c^+(\kappa^+) = f_0^+ + h \kappa^+ \quad (64)$$

where h is a material constant obtained from the uniaxial tensile stress-strain diagram. The evolution of the hardening parameters was shown in Eqs. (58) and (59).

The flow rule gives the relation between the plastic flow direction and the plastic strain rate. A non-associated flow rule means that the yield function f and the plastic potential F^p do not coincide, and therefore, the direction of the plastic flow is not normal to the yield surface. This is important for realistic modeling of the volumetric expansion (dilatancy) under compression for frictional materials such as concrete (see Cervenka and Papanikolaou, 2008). Using an associated flow rule for the type of yield surface shown in Eq. (60) gives an unrealistically high volumetric expansion in compression, which leads in some cases to an overestimated strength - peak stress (Chen and Han, 1988). Therefore, the shape of the concrete loading surface at any given point in a given loading state should be obtained by using non-associative plasticity. The plastic strain rate can be written in terms of the effective stress $\bar{\sigma}_{ij}$ as:

$$\dot{\epsilon}_{ij}^p = \dot{\lambda} \frac{\partial F^p}{\partial \bar{\sigma}_{ij}} \quad (65)$$

where $\dot{\lambda}$ is the plastic flow parameter (consistency factor) known as the Lagrangian multiplier, which can be obtained using the plasticity consistency condition, and the plastic potential function F^p takes the following Drucker-Prager format as given in Lee and Fenves (1998):

$$F^p = \sqrt{3J_2} + \alpha^p \bar{I}_1 \quad (66)$$

such that:

$$\frac{\partial F^p}{\partial \bar{\sigma}_{ij}} = \frac{3}{2} \frac{\bar{s}_{ij}}{\sqrt{3J_2}} + \alpha^p \delta_{ij} \quad (67)$$

where α^p is a parameter chosen to provide proper dilatancy with common range between 0.2 and 0.3 for concrete (Lee and Fenves, 1998; Wu et. al., 2006).

The plasticity consistency condition can be obtained by taking the time derivative of the plasticity yield function, $\dot{f} = 0$, and satisfying the following Kuhn-Tucker loading/unloading conditions:

$$\begin{aligned}
& \text{KuhnTucker } f \leq 0, \dot{\lambda}^p \geq 0 \rightarrow \dot{\lambda}^p f = 0 \\
& \text{Consistency } f = 0 \rightarrow \dot{\lambda}^p \dot{f} = 0 \\
& f < 0 \text{ then } \dot{\lambda}^p = 0 \text{ (elastic region)} \\
& f = 0 \text{ and } \dot{f} < 0 \text{ then } \dot{\lambda}^p = 0 \text{ (elastic unloading)} \\
& f = 0, \dot{f} = 0 \text{ and } \dot{\lambda}^p = 0 \text{ (neutral loading)} \\
& f = 0, \dot{f} = 0 \text{ and } \dot{\lambda}^p > 0 \text{ (plasticity)}
\end{aligned} \tag{68}$$

This concludes the plastic formulation for the present model. The damage formulation is discussed next where the tensile and compressive damage surfaces are defined.

6. Damage Formulation

The isotropic damage in this work is responsible for the softening response and the degradation in the elastic stiffness. The tensile and compressive damage surfaces and their hardening functions will be presented first, followed by a brief discussion of the damage consistency conditions.

To determine stress states during a damaging process from the thermodynamic constitutive relations, Eqs. (26), (28) b and (28)c, tensile and compressive damage surfaces and their evolution laws have to be specified. Referring to the definitions of a yield function and the plastic flow rule in plasticity theory, Tao and Phillips (2005) defined for an isothermal process the following two damage surfaces g^\pm as functions of the damage thermodynamic conjugate forces Y_{ij}^\pm and the scalar damage parameters φ^\pm , with a similar form to that of La Borderie et. al. (1992):

$$g^\pm = Y^\pm - Y_0^\pm - Z^\pm \leq 0 \text{ (no mixing } \pm) \tag{69}$$

where Y_0^\pm are initial damage thresholds (tension and compression) which govern the onset of tensile or compressive damage, respectively. As damage progresses, initial damage surfaces change by means of evolution laws defined by hardening/softening parameters Z^\pm . These parameters Z^\pm can be expressed mathematically in different forms, such as polynomials, power and exponential functions, etc. Amongst them power and exponential functions have the best match for the shapes of loading curves of concrete (Lubliner et. al., 1989; Lee and Fenves, 1998; Nechnech et. al., 2002; Tao and Phillips, 2005; Wu et. al., 2006 and others). Tao and Phillips (2005) assumed that the softening of damage surfaces follow a power law in the form of:

$$Z^\pm = \frac{1}{a^\pm} \left(\frac{\varphi^\pm}{1 - \varphi^\pm} \right)^{\frac{1}{b^\pm}} \tag{70}$$

in which a^\pm and b^\pm are four material constants to be calibrated by means of uniaxial tensile and compressive experiments of concrete. Tao and Phillips (2005) studied the effects of a^\pm and b^\pm on Z^\pm as damage progress. They showed that the shape of damage surface varies with b^\pm , whilst a^\pm determine the magnitude of Z^\pm . In other words, parameters a^\pm mainly dominate the magnitude of damage surfaces with units of MPa^{-1} , whilst b^\pm , being dimensionless parameters, influence generally the characteristics of softening/hardening (see Figure 1). The same trend was observed in this work as will be shown in the verification section. Tao and Phillips (2005) claimed that a proper selection of parameters a^\pm and b^\pm tailors Z^\pm to the demands of different types of concrete and their corresponding tensile and compressive strengths without the use of any regularization techniques. Other researchers that used Eq. (69) to model their isotropic damage criteria include Salari et. al. (2004), Shao et. al. (2006), and Grassl and Jirasek (2006). All three used single isotropic damage variable φ and thus, a single damage criterion.

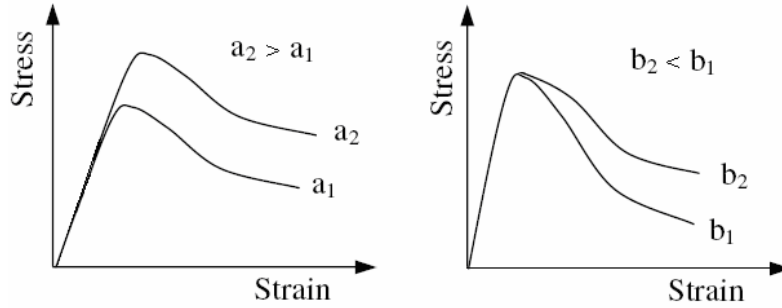


Figure 1: Effect of material parameters a^\pm and b^\pm on model behavior

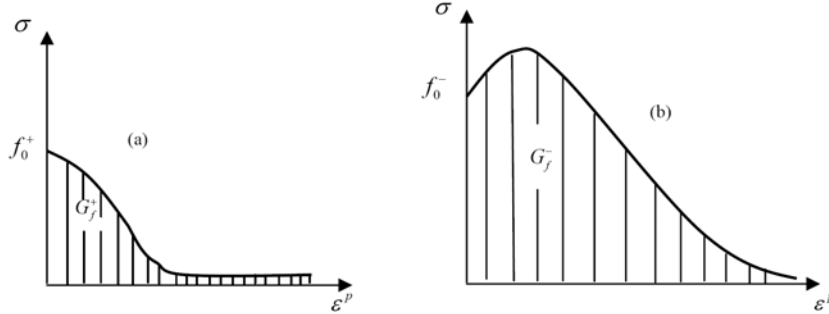


Figure 2: $(\sigma - \varepsilon^p)$ relation for uniaxial test, a) tension, b) compression

In this work, and in an effort to reduce the sensitivity of the FE analysis of concrete to the refinement of the FE meshes, the damage magnitude parameters a^\pm are adjusted to include dimensionless embedded coefficients γ^\pm that are related to the fracture energies in tension and compression, G_f^\pm (see Figure 2), and to the (geometrical) characteristic length, ℓ , of the applied FE mesh obtained from ABAQUS. These γ^\pm coefficients are given as (Oliver et. al., 1990; Labadi and Hannachi, 2005; Wu. et. al., 2006):

$$\gamma^\pm = \left[\frac{G_f^\pm \bar{E}}{\ell f_o^{\pm 2}} - \frac{1}{2} \right]^{-1} \tag{71}$$

A stress point in principal stress space can be either within or on the current damage surface. When within the damage surface, being tensile or compressive, the stress point may be loading, but it has not violated the current damage criterion yet. Once it is on the damage surface, two damage states are possible. One may be unloading or neutral loading, having $\dot{\phi}^\pm = 0$. The other is loading, accompanied by the evolution of damage and defined as $\dot{\phi}^\pm > 0$. Mathematically, the above description is expressed as:

$$\begin{aligned} \text{If } g^\pm < 0 & \quad \text{then } \dot{\phi}^\pm = 0; \\ \text{If } g^\pm = 0 \text{ and } \dot{g}^\pm \leq 0 & \quad \text{then } \dot{\phi}^\pm = 0; \\ \text{If } g^\pm = 0 \text{ and } \dot{g}^\pm = 0 & \quad \text{then } \dot{\phi}^\pm > 0 \end{aligned} \tag{72}$$

The above conditions are damage extension of the classical plasticity Kuhn–Tucker conditions (Voyiadjis and Kattan, 1992).

7. The Consistent Elastic – Plastic – Damage Tangent Operator

For the global equilibrium, solved by ABAQUS according to a Newton–Raphson algorithm, a consistent tangent operator is computed according to the procedures described in Jason et. al. (2006) and Wu et. al. (2006). It is formulated

by applying the derivative of the constitutive equation, Eq.(7), with respect to the strain tensor as follows (all parameters are at the (n+1) state):

$$\frac{\partial \sigma_{ij}}{\partial \varepsilon_{kl}} = (1 - \Phi) \frac{\partial \bar{\sigma}_{ij}}{\partial \varepsilon_{kl}} - \frac{\partial \Phi}{\partial \varepsilon_{kl}} \bar{\sigma}_{ij} \quad (73)$$

where the elasto-plastic consistent tangent operator appears in the first term on the right hand side of this equation. Since damage depends on the elastic strain only, $\frac{\partial \Phi}{\partial \varepsilon_{kl}}$ can be written as:

$$\frac{\partial \Phi}{\partial \varepsilon_{kl}} = \frac{\partial \Phi}{\partial \varepsilon_{mn}^e} \frac{\partial \varepsilon_{mn}^e}{\partial \varepsilon_{kl}} \quad (74)$$

and the derivative of the elastic strain tensor with respect to the total strain tensor can be obtained by taking the derivative of the constitutive equation, Eq. (3), with respect to the total strain tensor as follows:

$$\frac{\partial \varepsilon_{mn}^e}{\partial \varepsilon_{kl}} = (\bar{E}^{-1})_{mnpq} \frac{\partial \bar{\sigma}_{pq}}{\partial \varepsilon_{kl}} \quad (75)$$

Substituting Eqs. (74) and (75) into Eq. (73), the following arrangement can be obtained:

$$\frac{\partial \sigma_{ij}}{\partial \varepsilon_{kl}} = (1 - \Phi) \frac{\partial \bar{\sigma}_{ij}}{\partial \varepsilon_{kl}} - \frac{\partial \Phi}{\partial \varepsilon_{mn}^e} (\bar{E}^{-1})_{mnpq} \frac{\partial \bar{\sigma}_{pq}}{\partial \varepsilon_{kl}} \bar{\sigma}_{ij} \quad (76)$$

After some tensorial manipulations, Eq. **Error! Reference source not found.** can be given as:

$$\frac{\partial \sigma_{ij}}{\partial \varepsilon_{kl}} = \left[(1 - \Phi) \delta_{pi} \delta_{qj} - \frac{\partial \Phi}{\partial \varepsilon_{mn}^e} (\bar{E}^{-1})_{mnpq} \bar{\sigma}_{ij} \right] \frac{\partial \bar{\sigma}_{pq}}{\partial \varepsilon_{kl}} \quad (76)$$

Equation (76) is equivalent in format to that given by Wu et. al. (2006) as follows:

$$\frac{\partial \sigma_{ij}}{\partial \varepsilon_{kl}} = \left[\overbrace{(\delta_{pi} \delta_{qj})}^{\mathcal{L}} - \overbrace{(\Phi \delta_{pi} \delta_{qj})}^{\mathcal{O}} - \overbrace{\left(\frac{\partial \Phi}{\partial \varepsilon_{mn}^e} (\bar{E}^{-1})_{mnpq} \bar{\sigma}_{ij} \right)}^{\mathcal{R}} \right] \frac{\partial \bar{\sigma}_{pq}}{\partial \varepsilon_{kl}} \quad (77)$$

In order to obtain $\frac{\partial \sigma_{ij}}{\partial \varepsilon_{kl}}$, the derivative of the damage variable with respect to the elastic strain tensor, $\frac{\partial \Phi}{\partial \varepsilon_{mn}^e}$, needs to be evaluated. This can be accomplished by considering the derivative of Eq. (8) as follows:

$$\frac{\partial \Phi}{\partial \varepsilon_{mn}^e} = \frac{\|\bar{\sigma}_{ij}^+\|}{\|\bar{\sigma}_{ij}\|} \frac{\partial \varphi^+}{\partial \varepsilon_{mn}^e} + \frac{\|\bar{\sigma}_{ij}^-\|}{\|\bar{\sigma}_{ij}\|} \frac{\partial \varphi^-}{\partial \varepsilon_{mn}^e} \quad (78)$$

Note that the stresses in Eq. (8) are used to obtain scalar ratios that are used as weighing factors; therefore, they are not considered as contributing components to the foregoing derivative.

Substituting Eq. (70) into Eq. (69), explicit expressions for the damage variables (φ^\pm) satisfying the consistency conditions can be obtained as follows:

$$\varphi^\pm = \frac{(a^\pm [Y^\pm - Y_0^\pm])^{b^\pm}}{1 + (a^\pm [Y^\pm - Y_0^\pm])^{b^\pm}} = 1 - \frac{1}{1 + (a^\pm [Y^\pm - Y_0^\pm])^{b^\pm}} \quad (79)$$

It can be seen, using Eq. (79), that the damage variables φ^\pm are functions of the thermodynamic conjugate forces Y^\pm , respectively, and Y^\pm are functions of the elastic strain tensor ε_{mn}^e , Eqs. (48) and (49), such that the following expression can be obtained:

$$\frac{\partial \varphi^\pm}{\partial \varepsilon_{mn}^e} = \frac{\partial \varphi^\pm}{\partial Y^\pm} \frac{\partial Y^\pm}{\partial \varepsilon_{mn}^e} \quad (80)$$

The first term on the right hand side is obtained using Eq. (79) and given as:

$$\frac{\partial \varphi^\pm}{\partial Y^\pm} = \frac{a^\pm b^\pm (a^\pm [Y^\pm - Y_0^\pm])^{(b^\pm)-1}}{\left(1 + (a^\pm [Y^\pm - Y_0^\pm])^{b^\pm}\right)^2} \quad (81)$$

and the second term is obtained by applying the linearization technique given by (Simo and Hugues, 1998) using Eqs. (48) and (49) as follows:

$$\frac{\partial Y^\pm}{\partial \varepsilon_{mn}^e} = \frac{\frac{\|\bar{\sigma}_{ij}^\pm\|}{\|\bar{\sigma}_{ij}^\pm\|} \left(\bar{E}_{mnkl} \varepsilon_{kl}^e - \frac{1}{9} (1 - \chi^\pm) \varepsilon_{pp}^e \delta_{mn} \delta_{ij} \bar{E}_{ijkl} \delta_{kl} \right)}{1 - \frac{1}{2} \frac{\|\bar{\sigma}_{ij}^\pm\|}{\|\bar{\sigma}_{ij}^\pm\|} \left[\frac{c \exp(-dY^\pm) - c d Y^\pm \exp(-dY^\pm)}{(1 + c Y^\pm \exp(-dY^\pm))^2} \right]} \frac{1}{9} (\varepsilon_{qq}^e)^2 \delta_{ij} \bar{E}_{ijkl} \delta_{kl} \quad (82)$$

where the derivatives of χ^\pm with respect to the elastic strain tensor were expressed as follows:

$$\frac{\partial \chi^\pm}{\partial \varepsilon_{mn}^e} = \frac{\partial \chi^\pm}{\partial Y^\pm} \frac{\partial Y^\pm}{\partial \varepsilon_{mn}^e} \quad (83)$$

The effective consistent tangent operator $\frac{\partial \bar{\sigma}_{ij}}{\partial \varepsilon_{kl}}$ can be obtained using the linearization technique given in the references mentioned above and is stated here as given by Wu et. al. (2006) as:

$$\frac{\partial \bar{\sigma}_{ij}}{\partial \varepsilon_{kl}} = \left(\left(\bar{E}^{-1} \right)_{ijkl} + \frac{\partial F^p}{\partial \bar{\sigma}_{ij}} \frac{\partial \Delta \lambda^p}{\partial \bar{\sigma}_{kl}} + \Delta \lambda^p \frac{\partial^2 F^p}{\partial \bar{\sigma}_{ij} \partial \bar{\sigma}_{kl}} \right)^{-1} \quad (84)$$

where $\frac{\partial \Delta \lambda^p}{\partial \bar{\sigma}_{kl}}$ is given as:

$$\frac{\partial \Delta \lambda^p}{\partial \bar{\sigma}_{kl}} = - \frac{\frac{\partial f}{\partial \bar{\sigma}_{kl}}}{\frac{\partial f}{\partial \kappa^\pm} \left(\frac{\Delta \kappa^\pm}{\Delta \lambda^p} + \Delta \lambda^p \frac{\partial (\Delta \kappa^\pm / \Delta \lambda^p)}{\partial \hat{\sigma}_i} \frac{\partial \hat{\sigma}_i}{\partial \Delta \lambda^p} \right)} \quad (85)$$

where $\hat{\sigma}_i = \hat{\sigma}_{\max}$ when $\kappa = \kappa^+$ and $\hat{\sigma}_i = \hat{\sigma}_{\min}$ when $\kappa = \kappa^-$.

8. Verification of the Proposed Model

This section is dedicated to the numerical validation of the concrete model. The numerical algorithm of the proposed model, discussed in part II of this work, is implemented in the non-linear FE code ABAQUS via the user material subroutine UMAT. Several analytical examples are provided here in order to investigate the capability, applicability, and effectiveness of the proposed elastic-plastic-damage model in capturing material behavior in both tension and compression under uniaxial and bi-axial loadings. The results obtained by the proposed model are compared with corresponding experimental results to evaluate the model's performance. Tensile and compressive verification tests under uniaxial loading are demonstrated first, followed by biaxial tests in tension and compression.

8.1. Identification of the Proposed Model's Parameters

The proposed model contains 17 parameters: two elastic constants for the undamaged material (\bar{E} and $\bar{\nu}$), five parameters for the characterization of plasticity (α , α^p , h , Q and ω), eight parameters for damage characterization (a^\pm , b^\pm , Y_0^\pm , c and d), and two parameters for the fracture energy of concrete under tension and compression (G_f^\pm). All the parameters can be identified from a series of tensile and compressive experimental tests (Tao and Phillips, 2005 and Wu et. al., 2006). Since the elastic-plastic-damage model presented in this work is a combination of the effective elastic-plastic constitutive relations presented by (Lee and Fenves, 1998 and Wu et. al., 2006) and the damage model presented by (Tao and Phillips, 2005); the model parameters used in these works are used here with some adjustment to the damage parameters in order to take into consideration the plastic effect introduced in this work.

The initial elastic constants are determined from the linear part of stress–strain curves before the initiation of damage and plastic deformation (Shao et. al., 2006). For concrete materials, these averaged elastic parameters are documented in literature. The initial damage thresholds in tension and compression, Y_0^\pm , can be determined by locating the onset points of variation of elastic properties in the unloading paths (Tao and Phillips, 2005). As the damage evolution is coupled with plastic flow, it seems to be reasonable to consider that the damage initiation occurs at the same time as the plastic initiation under tensile loading. They are identified as the end of the linear part of the stress–strain curves in uniaxial tensile tests. Under compression, however damage start at an earlier stage than plasticity depending on the initial damage threshold Y_0^- . The plastic hardening parameters (Q and ω) are related to the saturated stress in the plastic regime and the rate of saturation.

Lee and Fenves (1998) and Wu et. al. (2006) used the following values for the elastic-plastic material parameters: Poisson's ratio $\bar{\nu} = 0.20$; the equibiaxial to uniaxial compressive strength ratio $f_{b0}^- / f_0^- = 1.16$, resulting with $\alpha = 0.12$ and the dilatancy parameter α^p was chosen as 0.20. Tao and Phillips, (2005), used the following values for the material parameters used to split the strain tensor into hydrostatic and deviatoric components: $c = 2.0 \text{ MPa}^{-1}$ and $d = 0.7 \text{ MPa}^{-1}$. These values are used throughout this work.

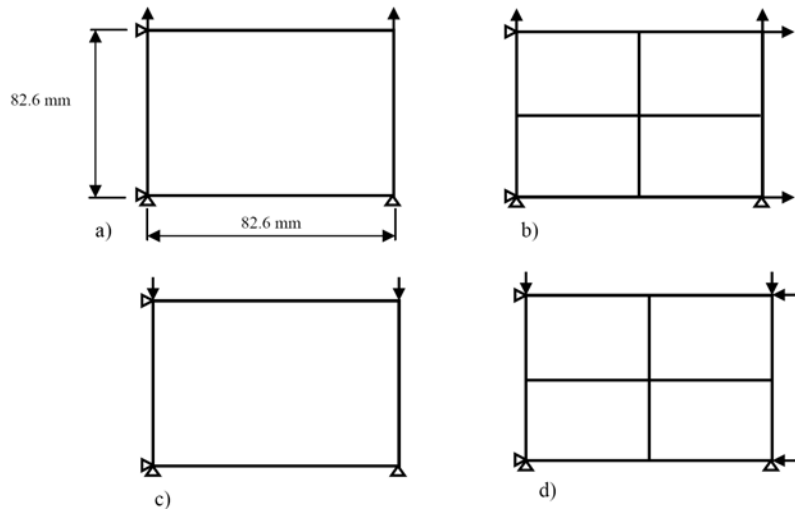


Figure 3: (a-d) Quadrilateral finite elements (CPS4 or CPE4) under uniaxial (a - tension, c - compression) and Biaxial (b - tension, d - compression)

8.2. Monotonic Uniaxial Tensile Test

In the first example of uniaxial tension test, the following material properties are used (Lee and Fenves, 1998; Tao and Phillips, 2005; Wu et. al., 2006; Nguyen and Houlsby, 2008a,b) in order to compare the results with the experimental work of Gopalaratnam and Shah (1985): $\bar{E} = 3.1 \times 10^4 \text{ MPa}$, $f_0^+ = 3.48 \text{ MPa}$ and $G_f^+ = 40 \text{ N/m}$. This test is conducted using a single quadrilateral finite element (82.6 mm x 82.6 mm) shown in Figure 3a to comply with the results of the studies mentioned above. The model's plastic hardening parameter is given here for the tensile case as: $h = 2.5 \times 10^4 \text{ MPa}$.

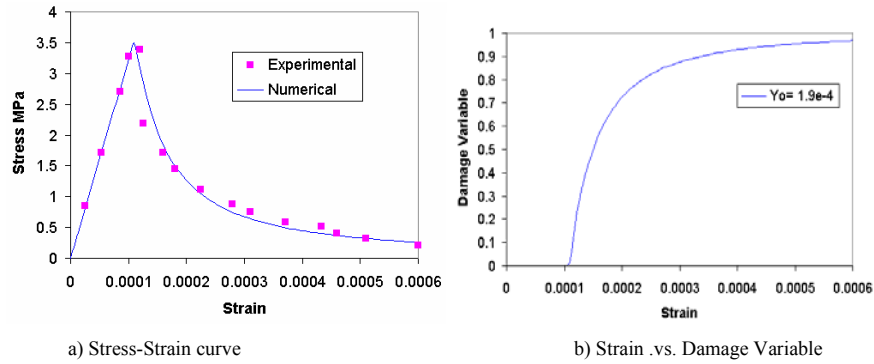


Figure 4: (a,b) The behavior of the proposed model under uniaxial tension

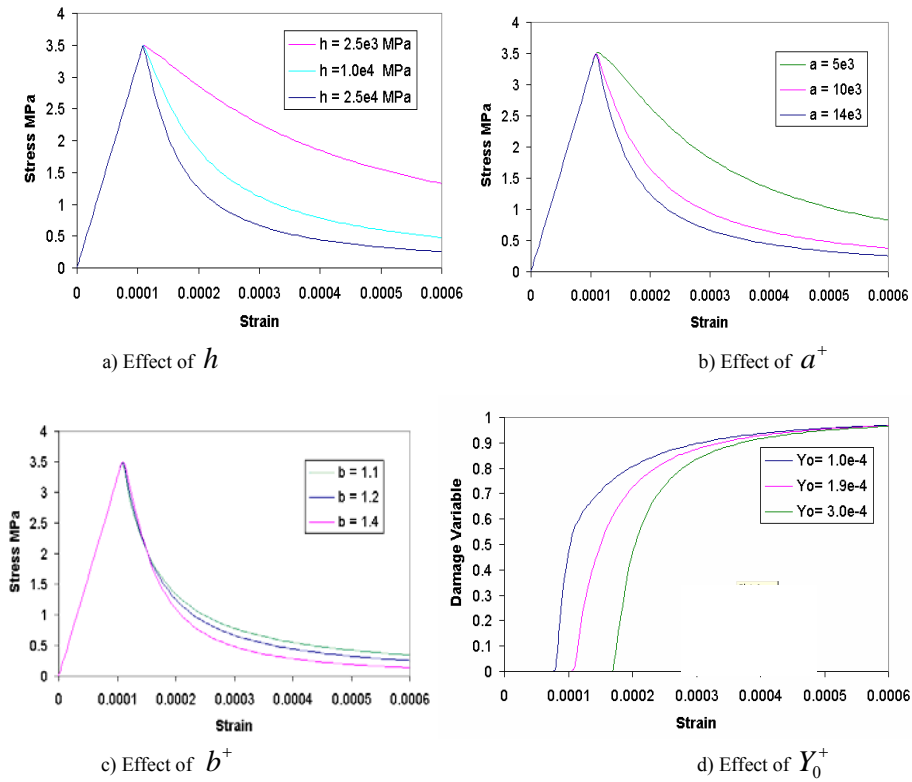


Figure 5: (a-d) Effect of material parameters on the model response in tension

The model's damage parameters are provided by Tao and Phillips, (2005) as: $b^+ = 1.2$, $Y_0^+ = 1.9 \times 10^{-4}$ MPa. Only parameter $a^+ = 14 \times 10^3$ MPa⁻¹ was adjusted to account for the plastic effect introduced in this work. Note that the uniaxial tests (in tension and compression) were used to determine the values of the material parameters to be used along with the fracture energy related factors γ^\pm in further examples. The use of the fracture energy factors γ^\pm in the verification problems is arbitrary and redundant as explained in (Nguyen and Houslyby, 2008a,b).

The stress-strain response is plotted in Figure 4a while damage evolution is plotted in Figure 4b. It can be observed from Figure 4a that the predictions obtained from the numerical model agree well with the experimental data (Gopalaratnam and Shah, 1985), especially for the post-peak nonlinear softening branches

The effect of the model parameters mentioned above on the stress-strain response and damage evolution in tension is shown in Figure 5a-d. Each model parameter in turn is varied, while others are kept fixed, to show the corresponding effect on the stress-strain curve and damage evolution.

Note in Figure 5a, that as the plastic hardening parameter h decreases, the plastic behavior becomes more dominant than the elastic one, resulting in smaller elastic strains, which affect the magnitude of the tensile damage release rate γ^+ and therefore negatively affect the damage growth. This shows the coupled effect of damage and plasticity on the predicted behavior.

8.3. Monotonic Uniaxial Compressive Test

The model's ability to reproduce the concrete behavior under monotonic uniaxial compression is verified here and compared to the experimental results of Karsan and Jirsa (1969). The material properties used here are (Lee and Fenves, 1998, Tao and Phillips, 2005; Wu et. al., 2006; Nguyen and Houlsby, 2008a,b): $\bar{E} = 3.1 \times 10^4$ MPa, $f_0^- = 10.2$ MPa, $f_c' = 27.6$ MPa and $G_f^- = 5690$ N/m. The test is conducted using a single quadrilateral finite element (82.6 mm x 82.6 mm) shown in Figure 3c. The model's plastic hardening parameters are given here for the compressive case as: $Q = 2.5 \times 10^3$ MPa and $\omega = 200$.

The model's damage parameters are provided as: $a^- = 22$ MPa $^{-1}$, $b^- = 0.98$, $\gamma_0^- = 3.0 \times 10^{-4}$ MPa $^{-1}$. The model's parameters a^- and b^- were adjusted in order to account for the introduction of the plastic effect in this work. The stress-strain response is plotted in Figure 6a while damage evolution is plotted in Figure 6b. Whether in the hardening or in the softening regimes, the overall nonlinear numerical performance predicted by the model and the experimentally obtained stress-strain curve are rather close.

The effect of model parameters on the stress-strain response and damage evolution in compression is shown in the Figure 7. Each model parameter in turn is varied, while others are kept fixed, to show the corresponding effect on the stress-strain curve and damage evolution; Figure 7a-d.

Figure 7b shows a trend similar to that observed in Figure 5a. As the magnitudes of the hardening parameters increase, the damage growth and thus the strain softening is more pronounced up to the point where the exponential hardening function becomes saturated. This again shows the coupled effect of damage and plasticity on the response of the proposed model.

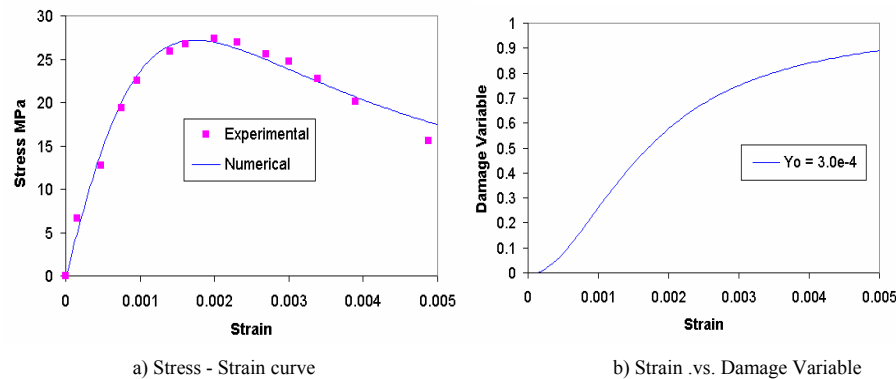


Figure 6: (a,b) The behavior of the proposed model under uniaxial Compression

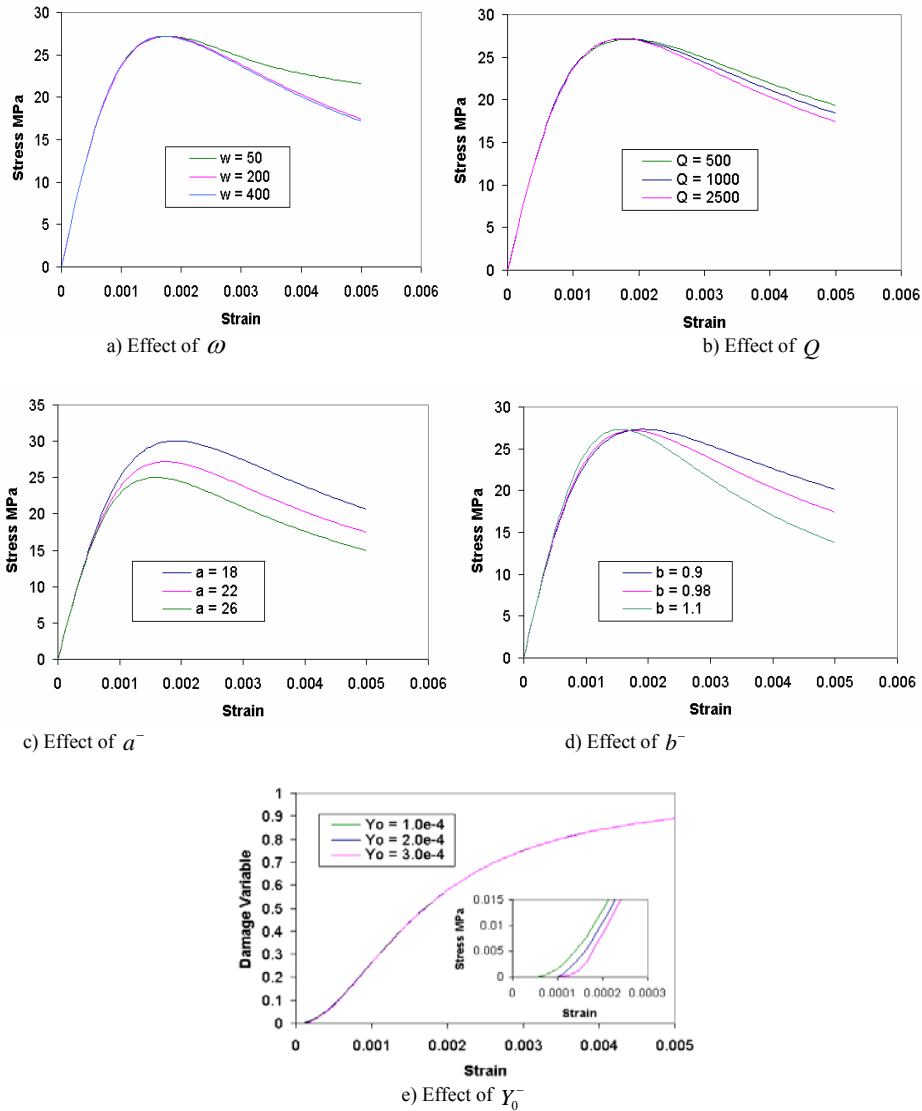


Figure 7: (a-e) Effect of material parameters on the model response in compression

8.4. Monotonic Biaxial Tests

In this section, the performance of the proposed model subjected to combined loading situations (biaxial tension, biaxial compression, and biaxial tension – compression) is investigated.

In the biaxial tension case, the same material parameters as those for the uniaxial tension test are used to analyze the Quadrilateral FE setup shown in Figure 3b. The numerical results are compared to the experimental ones reported by Kupfer et. al. (1969). In Figure 8a, the ordinate represents the normalized stress σ_{11} in terms of the compressive strength $f'_c = 27.6$ MPa for the case ($R = \sigma_{22} / \sigma_{11} = 1$). Note that the results of Kupfer et. al. (1969) cover only the range of ($0 \leq \sigma_{11} / f'_c \leq 0.09$). The results are in good agreement. The full range of the stress ratio ($0 \leq R \leq 1$) is investigated next.

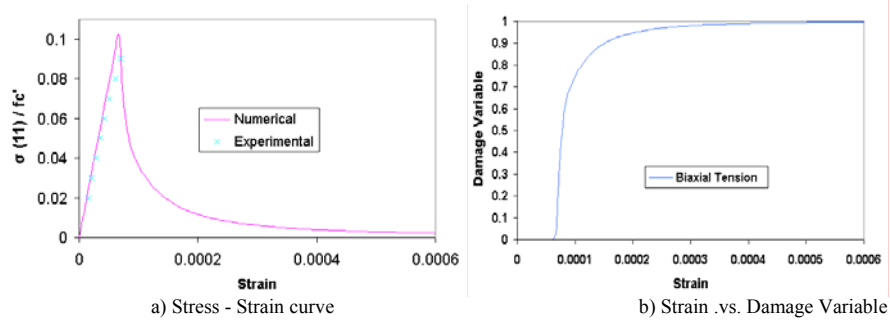


Figure 8: (a,b) The behavior of the proposed model under biaxial tension ($\sigma_{11} = \sigma_{22}$)

Table 1. Biaxial Tension Test

ϵ_{11}	ϵ_{22}	σ_{11}	σ_{22}	σ_{11} / f_c'	σ_{22} / f_c'
0.0006	0	3.48573	0	0.126295	0
0.0006	0.0001	3.48279	1.39312	0.126188	0.050475
0.0006	0.0002	3.39821	1.82981	0.123124	0.066297
0.0006	0.0003	3.29641	2.19761	0.119435	0.079624
0.0006	0.0004	3.14892	2.47415	0.114091	0.089643
0.0006	0.0005	2.94521	2.64054	0.106711	0.095672
0.0006	0.0006	2.80792	2.80792	0.101736	0.101736
0.0005	0.0006	2.64054	2.94521	0.095672	0.106711
0.0004	0.0006	2.47415	3.14892	0.089643	0.114091
0.0003	0.0006	2.19761	3.29641	0.079624	0.119435
0.0002	0.0006	1.82981	3.39821	0.066297	0.123124
0.0001	0.0006	1.39312	3.48279	0.050475	0.126188
0	0.0006	0	3.48573	0	0.126295

During the biaxial tension test, the total displacements in the horizontal and vertical directions of the setup shown in Figure 3b are specified in the input file. In order to retrieve the full spectrum of stress ratios ($0 \leq R \leq 1$), the displacement in one direction is fixed while the displacement in the other direction is incremented during multiple runs of the input file. The results are shown in Table 1.

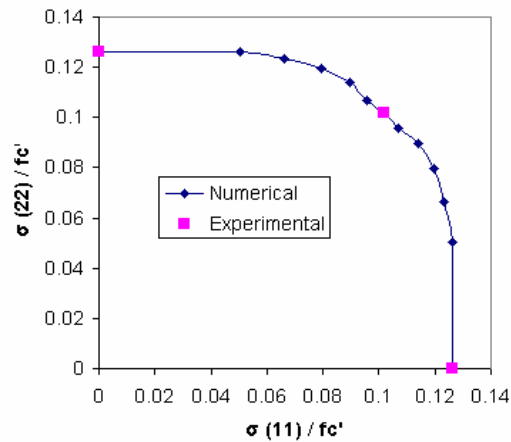


Figure 9: The biaxial tensile quadrant of the failure surface of concrete

The last two columns of Table 1 are plotted against each other to obtain Figure 9 showing the tensile quadrant of the biaxial failure surface of concrete. The experimental values were obtained by Kupfer et. al. (1969) and used by Lee and Fenves (1998) and Wu et. al. (2006).

The tensile biaxial results are compared to those of the uniaxial tension test. Figure 10a shows that under the biaxial state ($\sigma_{11} = \sigma_{22}$), the model predicts higher damage growth rate than under uniaxial tension. This is also obvious from Figure 10b, where damage starts at an earlier stage and grows at a higher rate.

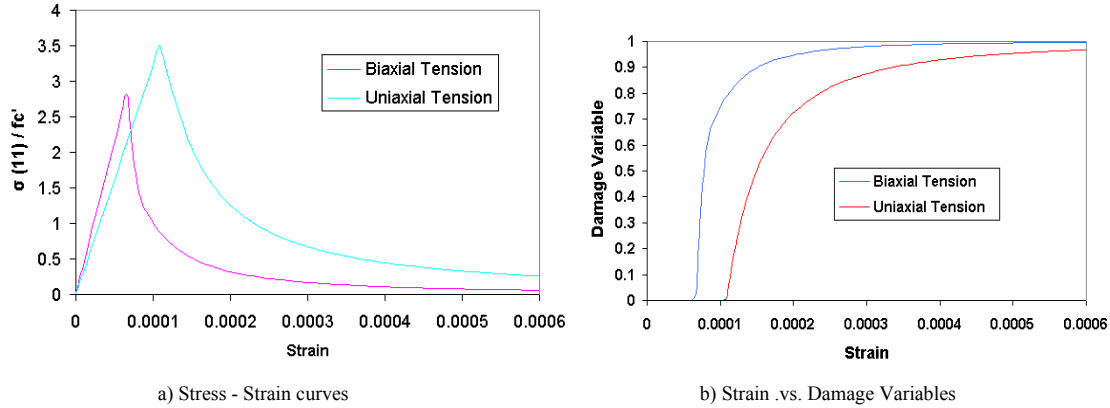


Figure10: a, b Comparison of the uniaxial and biaxial ($\sigma_{11} = \sigma_{22}$) tension tests

In the case of biaxial compression, the proposed model in its given form is not capable of capturing the trend observed experimentally. A modification that had to be applied to the proposed model in order to enhance its performance under biaxial compression is discussed next. This modification is easily incorporated into the UMAT file using proper IF statements. Experimental results (e.g. Kupfer et. al. (1969)) showed an increase in concrete compressive strength as the biaxial stress ratio ($R = \sigma_{22} / \sigma_{11}$) increases up to the point where the strength in one direction is $1.3 f_c'$, followed by a reduction in strength that reaches $1.16 f_c'$ when $R=1.0$ (see Figure 11). This is a result of the consolidation of concrete under biaxial compressive loading which leads to reduced damage growth (Wu et. al., 2006). This experimental observation is modeled here through the reduction of the damage encountered by concrete as the stress ratio R is increased. Since the compressive damage parameter a^- is responsible for the magnitude of damage endured by concrete as was shown in Figure 7c, this parameter is related to the biaxial strain ratio ($\varepsilon_{22} / \varepsilon_{11}$) in an effort to account for damage reduction during biaxial compressive loading in a displacement-controlled environment. The same material parameters as those used for the uniaxial compressive test are used here with $f_0^- = 15.2$ MPa (Wu et. al., 2006). The FE setup shown in Figure 3d was used.

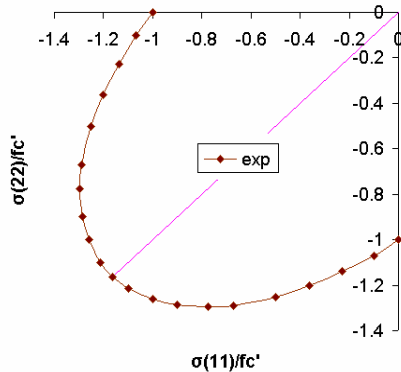


Figure 11: The biaxial compressive quadrant of concrete envelop (Kupfer et. al. 1969)

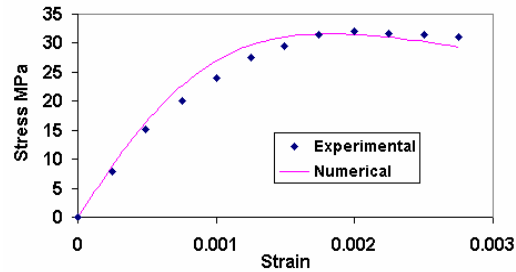


Figure 12: The behavior of the proposed model under biaxial compression ($\sigma_{11} = \sigma_{22}$)

Under Uniaxial compressive loading, the damage parameter $a^- = a_u^- = 22 \text{ MPa}^{-1}$ was shown to give good experimental fit (Figure 6a, $f'_c = 27.6 \text{ MPa}$). Whereas, under biaxial compression loading with a stress ratio of $R = 1$, $a^- = a_{eb}^- = 11 \text{ MPa}^{-1}$ was observed to give acceptable results ($f'_{bc} = 32 (1.16*27.6) \text{ MPa}$) as shown in Figure 12. The experimental results are those of Kupfer et. al. (1969).

It is worth mentioning here that the relation between damage growth and the damage parameter a^- is a proportional relation; the higher the value of a^- , the higher is the magnitude of damage. For example, if the damage magnitude is fixed at $\Phi = 0.3$, and a^- is increased from 11 to 22 MPa^{-1} , Figure 13a can be obtained to show the damage hardening function Z^- (MPa) plotted against a^- . Furthermore, if some arbitrary value is assigned to the damage release rate, say $Y^- = 0.01 \text{ MPa}$, and the value of a^- is increased from 11 to 22 MPa^{-1} again, then damage growth can be plotted against a^- as shown in Figure 13b.

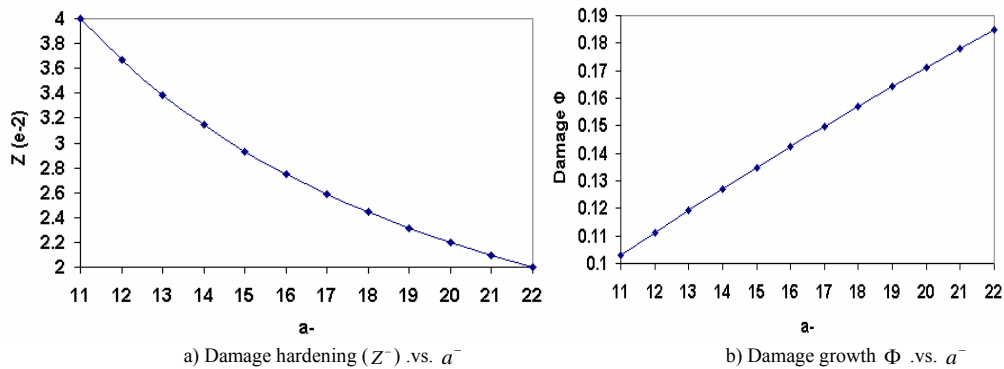


Figure 13: Relation between damage hardening (Z^-)/growth (Φ) and the damage hardening parameter a^-

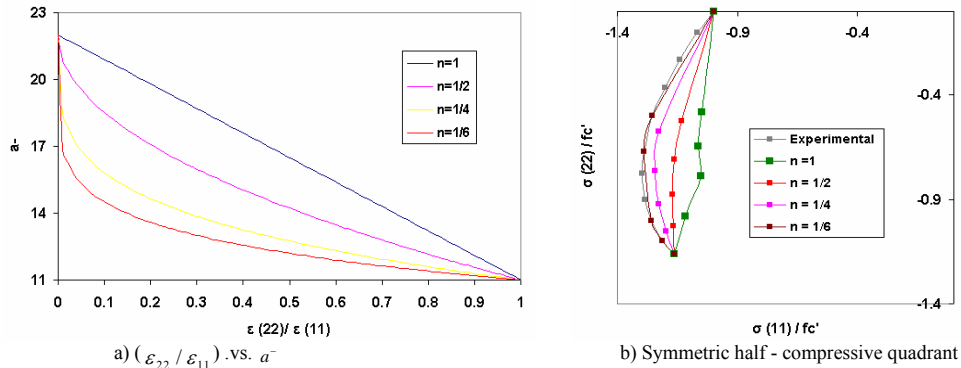


Figure 14: (a, b) The effect of $\epsilon_{22} / \epsilon_{11}$ on a^- and on the compression quadrant

By checking the biaxial compression stress envelop of concrete, Figure 11, one can easily see that when the stress ratio R is zero, the point on the envelop is $(-1, 0)$ and the consolidation effect doesn't exist. On the other hand, the consolidation effect starts to increase as R moves away from $(-1,0)$ towards higher values of R up to a certain point where the consolidation effect starts to decrease until the stress ratio $R=1$ is reached. By plotting the values of the strain ratio $\epsilon_{22} / \epsilon_{11}$ versus different power evolution equations of the damage parameter a^- , it was realized that the equation that best describes the evolution of a^- with respect to R is the one given as follows:

$$a^- = a_u^- - a_{eb}^- \left(\frac{\epsilon_{22}}{\epsilon_{11}} \right)^n \tag{86}$$

where a_u^- and a_{eb}^- are the compressive uniaxial and equibiaxial calibrated values of the damage parameter a^- . Figure 14a shows different curves for the evolution of a^- obtained by plotting Eq. (86) over the full range of the strain ratio $\varepsilon_{22} / \varepsilon_{11}$ using different values of the power parameter (n). Figure 14b, on the other hand, shows a symmetric half of the biaxial compressive quadrant of the concrete envelop. The results in Figure 14b are obtained by varying the horizontal and vertical displacements in the input file during multiple runs in order to obtain different stress ratios and their corresponding values of the damage variable a^- . Table 2 shows the numerical values for the series of runs used to obtain the curve representing (n = 1/6), which is the closest fit to experimental results reported by Kupfer et. al., (1969) as shown in Figure15.

Table 2 Biaxial Compression Test (n = 1/6)

$\varepsilon_{22} / \varepsilon_{11}$	σ_{11}	σ_{22}	$\sigma_{22} / \sigma_{11}$	σ_{11} / f'_c	σ_{22} / f'_c	a^-
0	-27.6	0	0	-1	0	22
0.055	-33.9815	-11.0433	0.32498	-1.23121	-0.40012	15.22063
0.14	-35.018	-13.9127	0.397301	-1.26877	-0.50408	14.09824
0.2	-35.3416	-15.9112	0.450212	-1.28049	-0.57649	13.58803
0.4	-35.297	-21.4989	0.609086	-1.27888	-0.77895	12.55788
0.6	-34.4252	-25.9382	0.753465	-1.24729	-0.93979	11.89776
0.8	-33.3097	-29.444	0.883947	-1.20687	-1.06681	11.40158
0.9	-32.7517	-30.9081	0.94371	-1.18666	-1.11986	11.19147
1	-32.1874	-32.1874	1	-1.16621	-1.16621	11

In the case of biaxial tension and compression, the model did not fit the experimental results, even with the modification used for the biaxial compression case mentioned above. The proposed model underestimates the strength of concrete under combined tension and compression (Figure 16). Varying the damage parameters a^+ and a^- with the strain ratio $\varepsilon_{22} / \varepsilon_{11}$ did not result in any improvements. This region of the concrete strength envelop still requires further research in order for the proposed model to adequately describe the biaxial tensile-compressive behavior of concrete. The results shown in Figure 16 were obtained by varying the magnitude of the damage release rates Y^\pm to account for the different tensile and compressive contributions to damage growth.

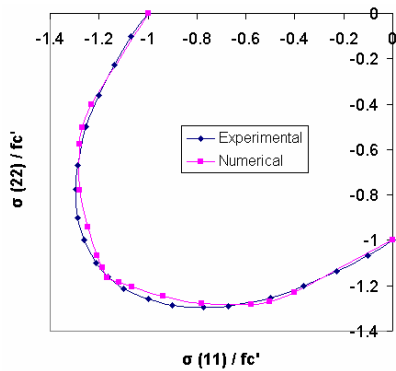


Figure 15: The biaxial compressive quadrant of the concrete envelop

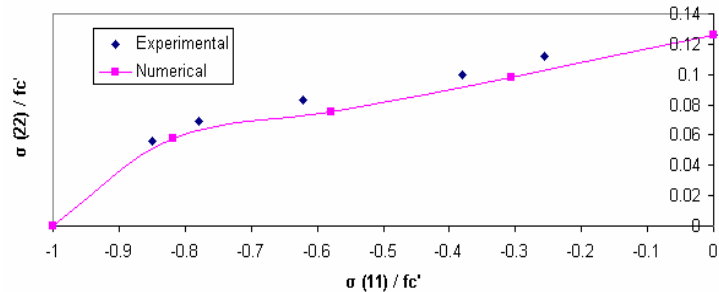


Figure 16: The mixed (tension/compressive) quadrant of the biaxial concrete envelop

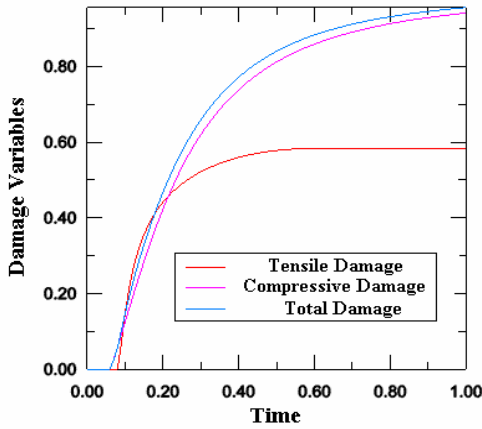


Figure 17: Tensile, compressive and total damage variables

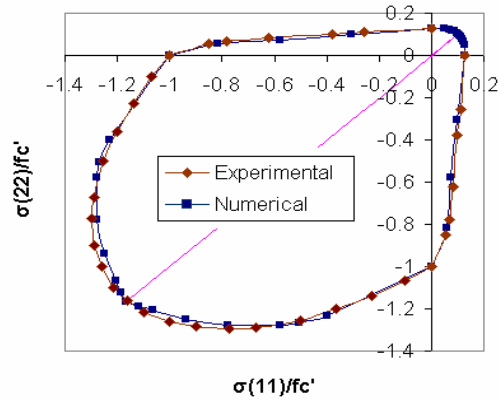


Figure 18: The biaxial strength envelop of concrete

Despite the difference between the numerical and experimental results observed in the mixed quadrants of the concrete envelop, it is worth mentioning that the combined damage variable Φ in these regions is made out of two parts, φ^+ and φ^- , unlike the other two quadrants (pure tensile or compressive quadrants). These two damage variables, φ^+ and φ^- , are combined using Eq. (8) to obtain the total damage variable Φ (Figure 17), where the latter is used to update the Cauchy stress tensor. Combining the results from different quadrants discussed above, the biaxial strength envelop of concrete can be plotted as shown in Figure 18. The experimental results pertain to Kupfer et. al., (1969).

8.5. Three Point Bending Test of a Notched Beam

In this section, the monotonic testing of the damaging process for a single-edge-notched plain concrete beam is simulated using experimental data from Malvar and Warren (1988). The square- illustrated in Figure 19a. The following material properties are used (Lowes, 1999; Lee and Fenves, 2001): $\bar{E} = 2.17 \times 10^4$ MPa, $f_c' = 29.0$ MPa, $f_0^+ = 2.4$ MPa, $G_f^+ = 35$ N/m. Two-dimensional cross-section beam, with an initial notch depth of 51 mm, is subjected to three-point loading test as FE mesh for the symmetric left part of the specimen is shown in Figure 19b. Displacement control is used to apply the loading in the simulation.

Applying the material parameters given above along with the characteristic length of the FE mesh given by ABAQUS as ($\ell = 12.6e^{-3}$ m) into Eq. (71), the mesh sensitivity parameter γ^+ can be calculated and the adjusted value for the damage parameter $a^+ = 1400$ MPa $^{-1}$ can be obtained. Since the elastic modulus, $\bar{E} = 2.17 \times 10^4$ MPa, in this test is lower than that considered in the uniaxial test, the tensile plastic hardening parameter h is reduced here to $h = 1.9 \times 10^4$ MPa to maintain the same ratio (h / \bar{E}).

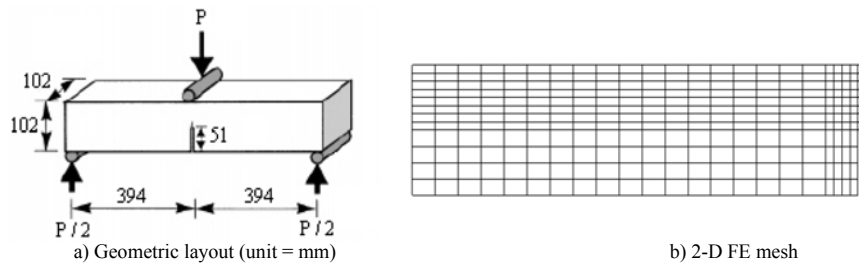


Figure 19:(a,b) Single-edge-notched beam subjected to three point bending test

In Figure 20, the load versus load-point deflection curve from the simulation is compared with the experimental result of Malvar and Warren (1988). Good agreement between the numerical and experimental results is observed, which demonstrates the effectiveness of the proposed model.

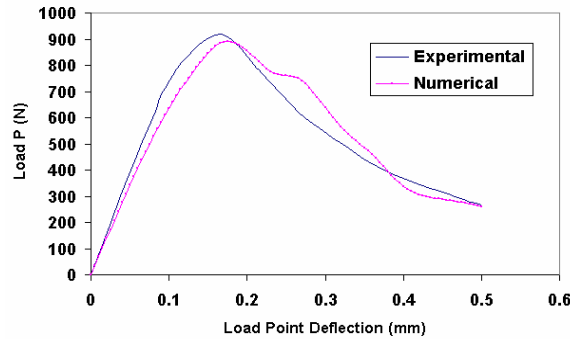


Figure 20: Load versus load-point deflection compared to experimental results

It should be noted here that the non-smoothness of the curve beyond the peak load is a phenomenon frequently observed in any numerical simulations that does not involve a regularization technique (Feenstra, 1993; Fichant et al., 1999; Lowes, 1999; Tikhomirov and Stein, 2001; Sumarac et al., 2003; Rabczuk et al., 2005; He et al., 2006; Nguyen and Houlsby, 2008a,b; Yu et al., 2008; and others). He et al. (2006) reported that the load-displacement curve beyond the maximum load and during the softening region, may reach a valley which is then followed by a new local peak in the next increment. These local peaks if not robustly tolerated and accounted for, will cause the algorithm to diverge.

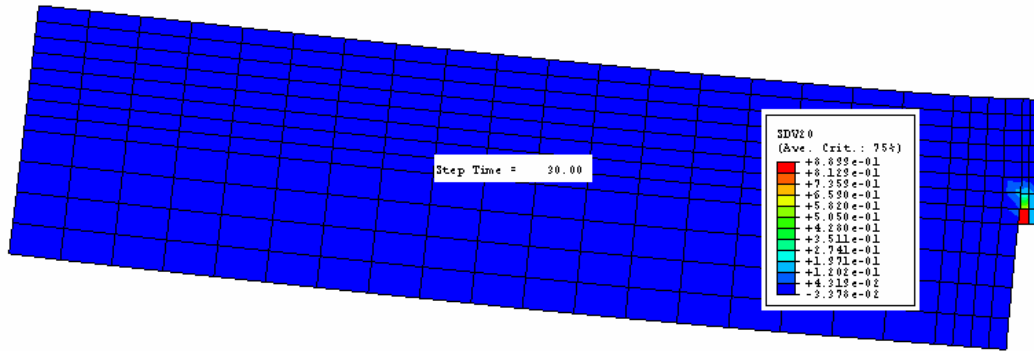
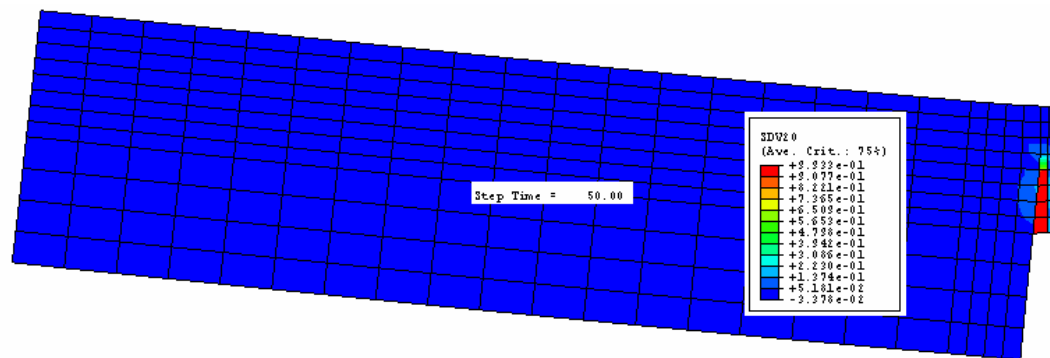
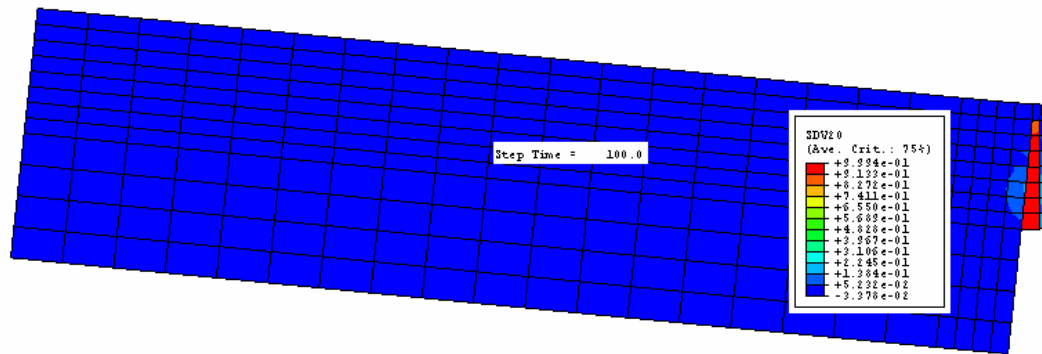
The evolution of damage is demonstrated next using the two dimensional FE mesh shown in Figure 19b. By applying a displacement control of -0.5 mm to the point of load application through 100 time increments, Figures. 21a-c show how damage propagates starting at the tip of the notch working its way toward the top of the cross-section. It should be noted here that the effect of the fracture energy parameters on reducing mesh sensitivity of the numerical results will be thoroughly investigated and discussed in part II of this work where reinforced concrete beams are studied using different mesh refinements.

9. Conclusions

This study introduces a continuum FE approach that is appropriate for predicting the physical behavior of concrete members subjected to short term monotonic loading assuming isothermal conditions. This approach consists of fracture energy based damage mechanics and plasticity theory adopted to describe the complex behavior of concrete material in structural elements.

The proposed material model for concrete is derived using rigorous and consistent thermodynamic formulation. The additive decomposition of the Helmholtz free energy concept is used to define the thermodynamic conjugate forces associated with the internal state variables, including the damage thermodynamic conjugate forces (damage energy release rates). The energy dissipation mechanisms are formulated to satisfy the first inequality of thermodynamics, and to postulate the plastic and damage dissipation functions. Three dissipation mechanisms (plasticity, tensile and compressive damage) are present to control the dissipation process of the material model.

The concrete model is a combination of the generalized effective space plasticity theory and isotropic damage theory applied simultaneously under the assumptions of small strains, rate independence, and isothermal conditions. The strain equivalence hypothesis is used for the stress mapping/transformation from the effective (undamaged) to the damaged configurations. A concrete plasticity yield function with multiple isotropic hardening criteria and a non-associative plasticity flow rule is adopted to represent the irreversible plastic behavior of concrete. The non-associative flow rule includes a hydrostatic term to account for the dilatation effect of concrete materials. On the other hand, two damage growth criteria that are based on the hydrostatic-deviatoric sensitive thermodynamic-conjugate forces are used to model stiffness degradation and material deterioration in concrete. Two damage variables, tensile and compressive, are used to model the different damaging behaviors in concrete. These two damage variables are combined using a relation that incorporates the stress tensor and its spectral decomposition into tensile and compressive components. The combined damage variable is consequently used to map the stress from the effective to the damaged configuration. Fracture energy related coefficients have been defined and incorporated in the damage model to achieve a reasonable degree of discretization insensitivity in numerical calculations. Their effect will be demonstrated and studied in part II of this work.

a) Evolution of damage (Φ) at 20 time incrementsb) Evolution of damage (Φ) at 50 time incrementsc) Evolution of damage (Φ) at 100 time incrementsFigure 21: a-c Evolution of damage (Φ) at different time increments

The proposed concrete model is implemented and tested to verify its capability, applicability, and effectiveness in capturing the material behavior in both tension and compression under uniaxial and bi-axial loadings. The results obtained by the proposed model are compared with corresponding experimental results to evaluate the model's performance. Tensile and compressive verification tests under uniaxial loading are demonstrated first, followed by biaxial tests in tension and compression. Then a three point bending test of a notched beam is investigated.

The numerical results of the verification examples under tensile and compressive uniaxial loads demonstrate the effectiveness of the model in capturing the uniaxial behavior of concrete. During all stages of loading, the simulated results match the experimental ones in terms of physical behavior. The experimentally observed softening branch of the stress-strain diagram under uniaxial loading (tension or compression) is reproduced efficiently.

Under biaxial tension, the model easily depicts the experimentally observed phenomenon; concrete strength suffers a reduction as the biaxial stress ratio is increased. Whereas, under biaxial compression, an additional equation

governing the damage variables is introduced in order to account for the strengthening of concrete due to consolidation under biaxial compression. This improvement leads to a more efficient numerical representation of the experimental results under biaxial compression.

The proposed concrete model in its current form is not capable of capturing the experimentally observed behavior under combined tensile and compressive loadings. The reduction in compressive strength was not observed numerically as the tensile stress is increased and vice versa. Further development of the model is therefore required in these regions of loading to enhance the numerically simulated results.

When a three point bending test of a single notched concrete beam is investigated, the computational algorithm demonstrated robustness in simulating the entire stress-strain diagram of concrete and the evolution of damage. Nevertheless, some difficulties are encountered: the non-smoothness in the numerical results beyond the peak point is believed to be related to the global equilibrium iterations. Another possible source is the use of non-associative plastic flow rule, where the direction of the plastic flow is not normal to the yield surface. It is well documented in literature that local damage approaches exhibit mesh sensitivity and non-smooth results in the softening region. Regularization methods should be incorporated in order to overcome such drawbacks.

References

- ABAQUS (2004) User Manual, version 6.4, ABAQUS Inc., Pawtucket, Rhode Island, 2004.
- Abu-Lebdeh, T.M. and Voyiadjis, G.Z. (1993). Plasticity-Damage model for concrete under cyclic multiaxial loading, *ASCE J. Eng. Mech.* **119(7)**, pp. 1465-1484.
- Bicanic, N. and Pearce, C. J. (1996). Computational aspects of a softening plasticity model for plain concrete, *Mech. of Cohesive-frictional Mat.* **1(1)**, pp. 75-94.
- Cervenka, J. and Papanikolaou, V. K. (2008). Three dimensional combined fracture-plastic material model for concrete, *Int. J. Plasticity*, available online, in press.
- Chen, F. W. and Han, D. J. (1988). Plasticity for structural engineers, *Springer-Verlag*, New York.
- Cicekli, U., Voyiadjis, G. Z. and Abu Al-Rub, R. K. (2007). A plasticity and anisotropic damage model for plain concrete, *Int. J. Plasticity* **23(10-11)**, pp. 1874-1900
- Coleman, B. D. and Gurtin, M. E. (1967). Thermodynamics with internal state variables, *J. Chem. Phys.* **47**, pp. 597-613.
- Comi C. and Perego U. (2001). Fracture energy based bi-dissipative damage model for concrete, *Int. J. of Solids and Struct.* **38(36)**, pp. 6427-6454.
- Contrafatto, L., Cuomo, M. (2006). A framework of elastic-plastic damaging model for concrete under multiaxial stress states, *Int. J. Plasticity* **22(12)**, pp. 2272-2300.
- Faria, R., Oliver, J. and Cervera, M. (1998). A strain-based plastic viscous-damage model for massive concrete structures, *Int. J. Solids and Struct.* **35(14)**, pp. 1533-1558.
- Feenstra, P.H. (1993). Computational aspects of biaxial stress in plain and reinforced concrete, Dissertation, Delft University, the Netherlands.
- Feenstra, P.H. and Borst, R.D. (1996). A composite plasticity model for concrete, *Int. J. of Solids and Struct.*, **33(5)**, pp. 707-730.
- Fichant, S., La Borderie, C. and Pijaudier-Cabot, G. (1999). Isotropic and anisotropic descriptions of damage in concrete structures, *Int. J. Mech. Cohesive Frictional Mater.* **4**, pp. 339-359.
- Gatuingt, F. and Pijaudier-Cabot, G. (2002). Coupled Gurson Plasticity and Damage Model for Concrete Structures in Dynamics, *15th ASCE Engineering Mechanics Conference*, June 2-5, Columbia University, New York, NY.
- Gopalratnam, V.S. and Shah, S.P. (1985). Softening response of plain concrete in direct tension, *ACI Journal*, **82**, pp. 311-323.
- Grassl, P. and Jirásek, M. (2006). Damage-plastic model for concrete failure, *Int. J. of Solids and Struct.* **43(22-23)**, pp. 7166-7196.
- Grassl, P., Lundgren, K. and Gylltoft, K. (2002). Concrete in compression: a plasticity theory with a novel hardening law, *Int. J. of Solids and Struct.* **39(20)**, pp. 5205-5223.
- Hansen, N. R. and Schreyer, H.L. (1994). A Thermodynamically Consistent Framework for Theories of Elastoplasticity Coupled with Damage, *Int. J. Solids and Struct.* **31(3)**, 359-389.
- He, W., Wu, Y. F., Liewand, K.M. and Wu, Z. (2006). A 2D total strain based constitutive model for predicting the behaviors of concrete structures, *Int. J. of Eng. Science* **44(18-19)**, pp. 1280-1303.
- Jefferson, A.D. (2003). Craft—a plastic damage contact model for concrete - I. Model theory and thermodynamic considerations, *Int. J. Solids Struct.* **40**, pp. 5973-5999.
- Ju, J. W. (1989). On energy-based coupled elasto-plastic damage theories: constitutive modeling and computational aspects, *Int. J. Solids and Struct.* **25(7)**, pp. 803-833.

- Júnior, F. S. and Venturini, W. S. (2007). Damage modelling of reinforced concrete beams, *Advances in Engineering Software* **38(8-9)**, pp. 538-546.
- Kachanov, L. M. (1958). On the creep fracture time, *Izv. Akad. Nauk USSR Otd. Tech* 8, 26-31 (in Russian).
- Karsan, I.D. and Jirsa, J.O. (1969). Behaviour of concrete under compressive loadings, *Journal of Structure Division ASCE* **95(12)**, pp. 2535-2563.
- Khan, A.R., Al-Gadhib, A.H. and Baluch, M.H. (2007). Elasto-damage Model for High Strength Concrete Subjected to Multiaxial Loading, *Int. J. of Damage Mech.* **16(3)**, pp. 361-398.
- Krätzig, W. B. and Pölling, R. (2004). An elasto-plastic damage model for reinforced concrete with minimum number of material parameters, *Computers & Structures* **82(15-16)**, pp. 1201-1215.
- Kupfer, H.B., Hildorf, H.K. and Rusch, H. (1969). Behavior of concrete under biaxial stresses, *ACI Journal* **66 (8)**, pp. 656-666.
- Labadi, Y. and Hannachi, N. E. (2005). Numerical Simulation of Brittle Damage in Concrete, *Strength of Materials*, pp. 268-281.
- La Borderie, C., Mazars, J. and Pijaudier-Cabot, G. (1992). Response of plain and reinforced concrete structures under cyclic loading, *ACI SIP* **134**, pp. 147-72.
- Lammer, H. and Tsakmakis, C. (2000). Discussion of coupled elastoplasticity and damage constitutive equations for small and finite deformations, *Int. J. Plasticity* **16**, pp. 495-523.
- Lee, J. and Fenves, G. L. (1998). A plastic-damage model for cyclic loading of concrete structures, *J. Eng. Mech., ASCE*, **124**, pp. 892-900.
- Lee, J. and Fenves, G. L. (2001). A return-mapping algorithm for plastic-damage models: 3-D and plane stress formulation, *Int. J. Num. Meth. Eng.*, **50**, pp. 487-506.
- Lowes, L. N. (1999). Finite Element Modeling of Reinforced Concrete Beam-Column Bridge Connections, Dissertation, University of California, Berkeley, California, USA.
- Lubliner, J. (1990). Plasticity theory, New York, MacMillan.
- Lubliner, J., Oliver, J., Oller, S. and Onate, E. (1989). A plastic-damage model for concrete, *Int. J. Solids Struct.*, **25(3)**, pp. 299-326.
- Luccioni, B., Oller, S. and Danesi R. (1996). Coupled plastic-damaged model, *Comp. Meth. in Applied Mech. and Eng.* **129(1-2)**, pp. 81-89.
- Luccioni, B.M. and Rougier, V.C. (2005). A plastic damage approach for confined concrete, *Computers & Structures* **83(27)**, pp. 2238-2256.
- Malvar, L. J. and Warren, G. E. (1988). Fracture energy for three-point-bend tests on single-edge-notched beams, *Exp. Mech.* **45**, pp. 266-272.
- Mazars, J. (1984). Application de la mécanique de l'endommagement au comportement non linéaire et a la rupture du béton de structure, Thèse de Doctorat d'Etat, L.M.T., Université Paris, France.
- Mazars, J. and Pijaudier-Cabot, G. (1989). Continuum damage theory - application to concrete, *J. Eng. Mech.* **115(2)**, pp. 345-365.
- Menzel, A., Ekh, M., Runesson, K. and Steinmann, P. (2005). A framework for multiplicative elastoplasticity with kinematic hardening coupled to anisotropic damage, *Int. J. Plasticity*, **21**, 397-434.
- Meschke, G. and Lackner, R. (1997). Anisotropic modeling of cracked concrete based on plasticity-damage theory, In: D.R.J. Owen et al. (Eds.), *Computational Plasticity*, CIMNE, Barcelona, pp. 1543-1550.
- Nechnech, W., Meftah, F. and Reynouard, J. M. (2002). An elasto-plastic damage model for plain concrete subjected to high temperatures, *J. of Eng. Struct.* **24(5)**, pp. 597-611.
- Nguyen, G. D. and Houlsby, G. T. (2008a). A coupled damage-plasticity model for concrete based on thermodynamic principles: Part I: model formulation and parameter identification, *Int. J. Numer. Anal. Meth. Geomec.* **32(4)**, pp. 353-389.
- Nguyen, G. D. and Houlsby, G. T. (2008b). A coupled damage-plasticity model for concrete based on thermodynamic principles: Part II: non-local regularization and numerical implementation, *Int. J. Numer. Anal. Meth. Geomec.* **32(4)**, pp. 391-413.
- Oliver, J., Cervera, M., Oller, S. and Lubliner, J. (1990). Isotropic damage models and smeared crack analysis of concrete, In: *Proc. 2nd Int. Conf. Comput. Aided Analysis Design Conc. Structures*, Zell am See, pp. 945-957.
- Oller, S., Onate, E., Oliver, J. and Lubliner, J. (1990). Finite element nonlinear analysis of concrete structures using a plastic damage model, *Eng. Fracture Mech.* **35(1-3)**, pp. 219-231.
- Ortiz, M. (1985). A constitutive theory for the inelastic behavior of concrete, *Mech. Mat.* **4(1)**, pp. 67-96.
- Park, H. and Kim, J. Y. (2005). Plasticity model using multiple failure criteria for concrete in compression, *Int. J. of Solids and Struct.* **42(8)**, pp. 2303-2322.
- Rabczuk, T., Akkermann, J. and Eibl, J. (2005). A numerical model for reinforced concrete structures, *Int. J. of Solids and Struct.* **42(5-6)**, pp. 1327-1354.

- Resende L. (1987). Damage mechanics constitutive theory for the inelastic behaviour of concrete, *Comput. Meth. Appl. Mech. Eng.* **60**, pp. 57–93.
- Salari, M. R., Saeb, S., Willam, K. J., Patchet, S. J. and Carrasco, R. C. (2004). A coupled elastoplastic damage model for geomaterials, *Comp. Meth. in Applied Mech. and Eng.* **193(27-29)**, pp. 2625-2643.
- Shao, J.F., Jia, Y., Kondo, D. and Chiarelli, A.S. (2006). A coupled elastoplastic damage model for semi-brittle materials and extension to unsaturated conditions, *Mech. of Mat.* **38(3)**, pp. 218-232.
- Shen, X., Yang, L. and Zhu, F. (2004). A Plasticity-based Damage Model for Concrete, *Adv. in Struct. Eng.* **7(5)**, pp. 461-467.
- Simo, J. C. and Honein, T. (1990). Variational Formulation, Discrete Conservation Laws, and Path-Domain Independent Integrals for Elasto-Viscoplasticity, *ASME, J. of App. Mech.* **57**, pp. 488-497.
- Simo, J. and Hughes, T. (1998). Computational inelasticity, Springer-Verlag, New York.
- Simo, J. C. and Ju, J. W. (1987a). Strain and stress-based continuum damage model. Part I: Formulation, *Int. J. Solids Struct.* **23(7)**, pp. 821-840.
- Simo, J. C. and Ju, J. W. (1987b). Strain and stress-based continuum damage model. Part II: Computational aspects, *Int. J. Solids Struct.* **25(7)**, pp. 841-869.
- Steinmann, P., Miehe, C., Stein, E., (1994). Comparison of different finite deformation inelastic damage models within multiplicative elastoplasticity for ductile materials, *Comput. Mech.* **13**, pp.458–474.
- Sumarac, D., Sekulovic, M. and Krajcinovic, D. (2003). Fracture of Reinforced Concrete Beams Subjected to Three Point Bending, *Int. J. of Damage Mech.* **12(1)**, pp. 31-44.
- Tao, X. and Phillips, D. V. (2005). A simplified isotropic damage model for concrete under bi-axial stress states, *Cement and Concrete Composites*, **27(6)**, pp. 716-726.
- Taqieddin, Z. N. (2008). Elasto-Plastic and Damage Modeling of Reinforced Concrete, Dissertation, Louisiana State University, Louisiana, USA.
- Tikhomirov, D. and Stein, E. (2001). Finite element computations of anisotropic continuum damage in reinforced concrete, *Computers & Structures*, **79(22-25)**, pp. 2249-2260.
- Voyiadjis, G. Z. and Abu Lebdeh, T. M. (1993). Damage model for concrete using bounding surface concept, *J. Eng. Mech.* **119(9)**, pp. 1865-1885.
- Voyiadjis, G. Z. and Abu Lebdeh, T. M. (1994). Plasticity model for concrete using the bounding surface concept, *Int. J. Plast.* **10(1)**, pp. 1-21.
- Voyiadjis, G. Z. and Kattan, P. I. (1992). A plasticity-damage theory for large deformations of solids. Part I: Theoretical formulation, *Int. J. Eng. Sci.* **30**, pp. 1089-1108.
- Voyiadjis, G. Z. and Kattan, P. I. (1999). Advances in damage mechanics: Metals and metal-matrix composites, *Elsevier*, Oxford.
- Voyiadjis, G. Z. and Kattan, P. I. (2006). Advances in Damage Mechanics: Metals and Metal Matrix Composites, with an Introduction to Fabric Tensors, *Second Edition*, *Elsevier*, Oxford.
- Voyiadjis, G. Z., Taqieddin, Z. N. and Kattan, P. I. (2008). Anisotropic Damage-Plasticity Model for Concrete, *Int. J. Plasticity*, available online, in press.
- Voyiadjis, G. Z., Taqieddin, Z. N. and Kattan, P. I. (2008). Theoretical Formulation of a Coupled Elastic-Plastic Anisotropic Damage Model for Concrete using the Strain Energy Equivalence Concept, *Int. J. of Damage Mech.*, in press.
- Willam, K., Rhee, I. and Beylkin, G. (2001). Multiresolution Analysis of Elastic Degradation in Heterogeneous Materials, *Meccanica*, **36(1)**, pp. 131-150.
- Willam, K., Rhee, I. and Xi, Y. (2003). Thermal degradation of heterogeneous concrete materials, Special issue on Durability, *J. Mat. Civil Eng. ASCE* **17(3)**, pp. 276-285.
- Wu, J. Y., Li, J. and Faria, R. (2006). An energy release rate-based plastic-damage model for concrete, *Int. J. of Solids and Struct.* **43(3-4)**, pp. 583–612.
- Yazdani, S. and Schreyer, H. L. (1990). Combined plasticity and damage mechanics model for plain concrete, *J. Eng. Mech. ASCE* **116(7)**, pp. 1435-1450.
- Yu, R. C., Ruiz, G. and Chaves, E. W.V. (2008). A comparative study between discrete and continuum models to simulate concrete fracture, *Eng. Fracture Mech.* **75**, pp. 117–127.